Journal of Computational Physics 228 (2009) 6037–6077

Contents lists available at ScienceDirect

Journal of Computational Physics

journal homepage: www.elsevier.com/locate/jcp

# Solid–fluid diffuse interface model in cases of extreme deformations

N. Favrie, S.L. Gavrilyuk *, R. Saurel

*Aix-Marseille University, Polytech Marseille, UMR CNRS 6595 IUSTI, also SMASH Project, INRIA, 5 rue E. Fermi, 13453 Marseille Cedex 13, France*

ARTICLE INFO

*Article history:*
Received 30 July 2008
Received in revised form 5 May 2009
Accepted 5 May 2009
Available online 18 May 2009

*Keywords:*
Diffuse solid–fluid interfaces
Shocks
Hyperelasticity
Riemann problem
Godunov type methods

ABSTRACT

Diffuse interface methods have been recently proposed and successfully used for accurate compressible multi-fluid computations Abgrall [1]; Kapila et al. [20]; Saurel et al. [30]. These methods deal with extended systems of hyperbolic equations involving a non-conservative volume fraction equation and relaxation terms. Following the same theoretical frame, we derive here an Eulerian diffuse interface model for elastic solid-compressible fluid interactions in situations involving extreme deformations. Elastic effects are included following the Eulerian conservative formulation proposed in Godunov [16], Miller and Colella [23], Godunov and Romenskii [17], Plohr and Plohr [27] and Gavrilyuk et al. [14]. We apply first the Hamilton principle of stationary action to derive the conservative part of the model. The relaxation terms are then added which are compatible with the entropy inequality. In the limit of vanishing volume fractions the Euler equations of compressible fluids and a conservative hyperelastic model are recovered. It is solved by a unique hyperbolic solver valid at each mesh point (pure fluid, pure solid and mixture cell). Capabilities of the model and methods are illustrated on various tests of impacts of solids moving in an ambient compressible fluid.



## 1. Introduction

Solid–fluid interaction in cases of extreme deformations occurs in many fundamental and industrial applications: astrophysics with hypervelocity impacts and crater formations, nuclear engineering with solid–fluid instabilities in inertial fusion, non-Newtonian flows of jelly, civil engineering with concrete flows and others. In such extreme conditions it is often supposed that the stress tensor in solids is approximately spherical. The problem then reduces to a fluid–fluid interaction. However, to cover a wider domain of applications, it is necessary to develop a general mathematical model ranging from solid behavior, eventually highly non-linear elastic, to hydrodynamic behavior, with eventual compressible effects. This poses serious theoretical and numerical challenges:

- The building of a thermodynamically consistent conservative Eulerian non-linear elastic model. This issue has been addressed in Godunov [16], Miller and Colella [23], Godunov and Romenskii [17], Plohr and Plohr [27], Gavrilyuk et al. [14].
- The building of an algorithm able to handle solid–fluid interface conditions. This second issue is usually addressed by Lagrangian methods, or ALE methods that forbid numerical diffusion at solid–fluid interfaces. This type of method is widely used in the computation of solid–fluid interactions (see, for example, a pioneering paper by Wilkins [37]).

* Corresponding author.
*E-mail addresses:* nicolas.favrie@polytech.univ-mrs.fr (N. Favrie), sergey.gavrilyuk@polytech.univ-mrs.fr (S.L. Gavrilyuk), richard.saurel@polytech.univ-mrs.fr (R. Saurel).

0021-9991/$ - see front matter © 2009 Elsevier Inc. All rights reserved.
doi:10.1016/j.jcp.2009.05.015

Their Lagrangian character limits their applicability to finite deformations. For extreme deformations, Eulerian approaches are preferred. Interface reconstruction methods of VOF type [18] were used in Miller and Colella [23]. Level set methods have been used in Fedkiw [11] for the coupling of Lagrangian solid computations to Eulerian fluid description.

In the present paper, a diffuse interface method is built to describe solid–fluid coupling. In general, two approaches are used for description of diffuse interfaces. The first one is a Cahn–Hilliard type method, where the internal energy depends on the gradient of an order parameter describing the position of the interface separating different phases (see, for example Cottet et al. [8] where such a method was used for the interfaces separating an incompressible fluid and an incompressible solid). When strong compressibility effects are taken into account, a second approach is preferable. This class of models is reminiscent of multiphase flow models [5,20,33]. The interface position is determined by an order parameter which has a clear physical meaning (the volume or mass fraction of components). In the bulk phase ("far" from the interface), a negligible quantity of the second phase is present. In particular, this allows to avoid the degeneracy of the model. Also, boundary conditions between two phases (solid–gas, for example) are naturally implemented in the model formulation. Usually, this model is hyperbolic, and this guarantees the wellposedness of the Cauchy problem. This type of hyperbolic models was extensively used for fluid–fluid interaction problems with, eventually, phase transitions and chemical reactions. The advantages of such an approach are:

- The same numerical algorithm is used everywhere: in pure fluids and in mixture zones. The corresponding hyperbolic solvers with stiff mechanical relaxation are able to deal with interfaces separating pure compressible fluids [28].
- These methods are also able to deal with interfaces separating mixtures of materials, e.g. in the computation of detonation waves is condensed explosives where chemical decomposition produces multiphase mixtures of materials [7].
- These models and methods are able to dynamically create interfaces which are not present initially, e.g. in cavitation or spallation phenomena where gas pockets dynamically appear [21,29,30].

In the present paper we extend a similar approach to the solid–fluid coupling problem. Special attention is paid to the derivation of the flow model. It is derived in two steps. First, we formulate a constrained Lagrangian for a solid–fluid mixture modelling the interface, and derive non-dissipative hyperbolic equations of motion by using the Hamilton principle of stationary action. Mixture cells are considered as multiphase mixtures evolving in mechanical equilibrium but out of thermal equilibrium. Elasticity effects are included following the Eulerian conservative formulation proposed in Gavrilyuk et al. [14]. Then, the dissipation terms are introduced in a compatible way with the entropy inequality. The numerical solver also has to be developed carefully as:

- The fluid and solid equations of state are very different. In particular, geometrical equations describing the evolution of local cobasis vectors (or, what is equivalent, the evolution of the deformation gradient) are present in solids in order to determine the stress tensor. These equations are absent for fluids.
- Volume fraction positivity is particularly important as the material equations of state have limited range of validity, that may yield to negative pressures.
- Shock wave propagation and transmission through material interfaces is important as the materials are compressible.
- Interface conditions are different in fluids and in solids. In particular tangential sliding is allowed in fluids and forbidden in solids at contact discontinuities.
- Cavitation and spallation under expansion waves may occur in condensed materials.

The paper is organized as follows. The Eulerian formulation of elastic compressible materials and compressible fluids is recalled in Section 2. In Section 3 we derive a one-velocity diffuse interface equilibrium multiphase flow model for a solid–fluid coupling. The model admits sliding at solid–fluid interfaces. A hyperbolic pressure non-equilibrium model is then derived compatible with the entropy inequality. This model, even if apparently more complex, is easier to solve, in particular regarding to the Riemann problem solution and the volume fraction positivity. The numerical approximation of this model is developed in Section 4, as an extension of Saurel et al. [30] method for multi-fluid flows. One-dimensional test validations are given in Section 5. In Section 6 we present multi-dimensional examples, illustrating the method for flows under extreme deformations.

## 2. Generality for nonlinear elastic bodies and compressible fluids

### 2.1. Mathematical model of elastic bodies

Let $\mathbf{X} = (X^\beta), \beta = 1,2,3$, be the Lagrangian coordinates, $\mathbf{x} = (x^i), i = 1,2,3$ be the Eulerian coordinates. The motion of a solid is a diffeomorphism from the reference configuration $\Omega_0$ to the actual configuration $\Omega_t$:

$$\mathbf{x} = \boldsymbol{\phi}(t, \mathbf{X}).$$

The inverse difffeomorphism will be denoted by $\boldsymbol{\phi}^{-1}$. The deformation gradient is

$$F(t, \mathbf{X}) = \frac{\partial \boldsymbol{\phi}}{\partial \mathbf{X}} = \frac{\partial \mathbf{x}}{\partial \mathbf{X}}.$$

It can be always considered as a function of the Eulerian coordinates by using the composition of two mappings:

$$F(t, \boldsymbol{\phi}^{-1}(t, \mathbf{x})).$$

By an abuse of notation that simplifies the analysis, we shall use the same symbol $F$ for this composition. The same remark is about other variables which will be defined later. Also, the classical differential operators $\nabla$, div and rot are always applied to functions defined in the Eulerian coordinates. Let $G$ be the Finger tensor (the inverse to the left Cauchy–Green deformation tensor $C^L = FF^T$):

$$G = (C^L)^{-1} = (F^T)^{-1} F^{-1}.$$

We introduce a natural *curvilinear basis*

$$\mathbf{e}_\beta = \frac{\partial \boldsymbol{\phi}}{\partial X^\beta} = \frac{\partial \mathbf{x}}{\partial X^\beta}, \quad \beta = 1, 2, 3,$$

and a dual *curvilinear cobasis* (see Fig. 1)

$$\mathbf{e}^\beta = \nabla X^\beta, \quad \beta = 1, 2, 3.$$

The scalar product of these vectors satisfies

$$\mathbf{e}_\beta \cdot \mathbf{e}^\gamma = \delta^\gamma_\beta,$$

where $\delta^\gamma_\beta$ are the Kronecker symbols.

With these definitions

$$G = \sum_{\beta=1}^{3} \mathbf{e}^\beta \otimes \mathbf{e}^\beta. \tag{1}$$

The inverse tensor $G^{-1}$ will be then

$$G^{-1} = \sum_{\beta=1}^{3} \mathbf{e}_\beta \otimes \mathbf{e}_\beta.$$

The tensor $G$ will be used to describe the deformation of solid bodies (see Fig. 2). The Lagrangian coordinates considered as functions of the Eulerian coordinates conserve along the trajectories:

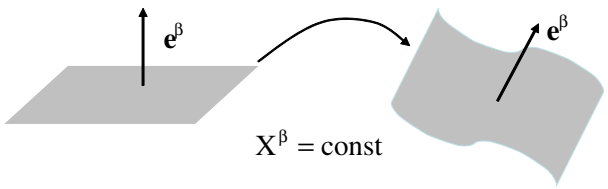


**Fig. 1.** Time evolution of the surfaces $X^\beta = const, \beta = 1, 2, 3$ is shown. The particles form at time $t = 0$ a plane $X^\beta = const$. The vector $\mathbf{e}^\beta$ is orthogonal to the surface $X^\beta = const$.

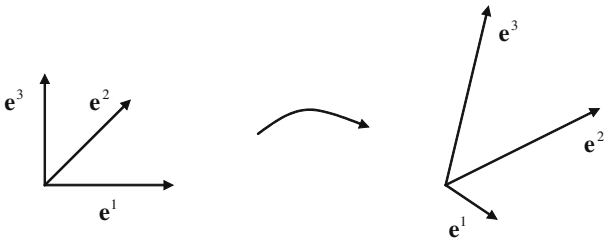


**Fig. 2.** Time evolution of the local cobasis vectors $\mathbf{e}^\beta, \beta = 1, 2, 3$ is shown. At time $t = 0$ they form the 3D Cartesian basis.

$$\frac{DX^\beta}{Dt} = 0, \quad \frac{D}{Dt} = \frac{\partial}{\partial t} + \mathbf{v}\cdot\nabla, \tag{2}$$

where $\mathbf{v}$ is the velocity field. By taking the gradient of (2) we obtain:

$$\frac{\partial \mathbf{e}^\beta}{\partial t} + \nabla(\mathbf{v}\cdot\mathbf{e}^\beta) = \mathbf{0}. \tag{3}$$

The stationary constraint following from the definition of $\mathbf{e}^\beta$

$$\mathrm{rot}\mathbf{e}^\beta = \mathbf{0}, \tag{4}$$

allows us to rewrite the evolution equation for the cobasis vectors in non-conservative form [14,16,17,23]:

$$\frac{\partial \mathbf{e}^\beta}{\partial t} + \nabla(\mathbf{v}\cdot\mathbf{e}^\beta) = -\mathrm{rot}\mathbf{e}^\beta \wedge \mathbf{v}. \tag{5}$$

For the vector $\mathbf{w}^\beta = \mathrm{rot}\mathbf{e}^\beta$ we obtain the following linear equation:

$$\frac{\partial \mathbf{w}^\beta}{\partial t} + \mathrm{rot}(\mathbf{w}^\beta \wedge \mathbf{v}) = 0. \tag{6}$$

It follows from (6) that if $\mathbf{w}^\beta = \mathrm{rot}\mathbf{e}^\beta = 0$ at $t = 0$, it will be zero for all time. However, numerically it is not so. A numerical strategy based on the parabolic regularization of (6) that control the gauge constraint $\mathbf{w}^\beta = 0$ in solids was developed in Miller and Colella [23] and Miller and Colella [24]. In the paper of Babii et al. [4] a different strategy has been proposed to resolve, in particular, the stationary constraints for the Maxwell equations, linear elasticity and magnetohydrodynamics. Analytically, the method consists in a resolution of an overdetermined system of equations where new unknowns (called "potentials") and the corresponding evolution equations are introduced. This approach can also be adapted to the non-linear pure solid model.

We present first the equations of *hyperelastic* bodies we will study. Recall that a material is *hyperelastic* if the stress tensor is defined in terms of a stored energy function. The equations of motion of hyperelastic isotropic solid bodies are written in the form [14,16,17,23]:

$$\frac{\partial \rho_s}{\partial t} + \mathrm{div}(\rho_s \mathbf{v}) = 0, \quad \rho_s = \rho_{s0}|G|^{1/2}, \quad \frac{D\rho_{s0}}{Dt} = 0, \tag{7a}$$

$$\frac{\partial \mathbf{e}^\beta}{\partial t} + \nabla(\mathbf{v}\cdot\mathbf{e}^\beta) = -\mathrm{rot}\mathbf{e}^\beta \wedge \mathbf{v}, \quad \mathrm{rot}\mathbf{e}^\beta = 0, \tag{7b}$$

$$\frac{\partial \rho_s \mathbf{v}}{\partial t} + \mathrm{div}(\rho_s \mathbf{v}\otimes\mathbf{v} - \sigma_s) = 0, \tag{7c}$$

$$\frac{\partial}{\partial t}\left(\rho_s\left(e_s + \frac{\mathbf{v}\cdot\mathbf{v}}{2}\right)\right) + \mathrm{div}\left(\rho_s\mathbf{v}\left(e_s + \frac{\mathbf{v}\cdot\mathbf{v}}{2}\right) - \sigma_s\mathbf{v}\right) = 0, \tag{7d}$$

where the specific energy of elastic body $e_s(G,\eta_s)$ verifies the Gibbs identity

$$\theta_s d\eta_s = de_s - tr\left(\frac{\partial e_s}{\partial G}dG\right) = de_s + \frac{1}{2\rho_s}tr(\sigma_s G^{-1}dG), \quad \sigma_s = -2\rho_s\frac{\partial e_s}{\partial G}G. \tag{8}$$

Here, $\eta_s$ is the entropy, $\theta_s$ is the temperature, $\rho_s$ is the density, $|G|$ is the determinant of $G$ defined by (1), $\rho_{s0}$ is the reference density which is, *a priori*, a function of Lagrangian coordinates, and $\sigma_s$ is the stress tensor. The components of the symmetric tensor $\frac{\partial e_s}{\partial G}$ are defined as follows

$$\left(\frac{\partial e_s}{\partial G}\right)_{ij} = \frac{\partial e_s}{\partial G_{ji}} = \frac{\partial e_s}{\partial G_{ij}}, \quad G_{ij} = \sum_{\beta=1}^{3}(\mathbf{e}^\beta)_i(\mathbf{e}^\beta)_j, \quad i,j = 1,2,3.$$

For isotropic elastic bodies the energy $e_s$ depends only on the invariants $J_m = tr(G^m), m = 1,2,3$ and the entropy $\eta_s$. In particular it implies that $\sigma_s$ is symmetric. Indeed,

$$\begin{aligned}\sigma_s &= -2\rho_s\frac{\partial e_s}{\partial G}G = -2\rho_s\left(\frac{\partial e_s}{\partial J_1}I + 2\frac{\partial e_s}{\partial J_2}G + 3\frac{\partial e_s}{\partial J_3}G^2\right)G = -2\rho_s G\left(\frac{\partial e_s}{\partial J_1}I + 2\frac{\partial e_s}{\partial J_2}G + 3\frac{\partial e_s}{\partial J_3}G^2\right) = -2\rho_s G\frac{\partial e_s}{\partial G}\\ &= -2\rho_s G^T\left(\frac{\partial e_s}{\partial G}\right)^T = \sigma_s^T.\end{aligned}$$

Governing equations of hyperelastic solid bodies have a variational formulation with the Lagrangian

$$L_s = \int_{\Omega_t}\rho_s\left(\frac{\mathbf{v}\cdot\mathbf{v}}{2} - e_s(G,\eta_s)\right)d\Omega,$$

where the mass, entropy and local cobasis equations should be considered as differential constraints [14,16]. It is useful to take the specific energy $e_s$ in separate form

$$e_s(G,\eta_s) = \varepsilon_s^h(\rho_s,\eta_s) + \varepsilon_s^e(\widetilde{G},\eta_s), \quad \widetilde{G} = \frac{G}{|G|^{1/3}}. \tag{9}$$

The hydrodynamic part $\varepsilon_s^h$ depends only on the density and the entropy. The elastic part $\varepsilon_s^e$ is a homogeneous function of zero degree with respect to $G$, it is unchanged during uniform compression because

$$|\widetilde{G}| = 1.$$

An important consequence of this is that the pressure $p_s$ in such a system is defined only by the hydrodynamic part of the energy $\varepsilon_s^h(\rho_s,\eta_s)$. The deviatoric part of the stress tensor is defined only by the elastic part of the energy $\varepsilon_s^e(\widetilde{G},\eta_s)$. For applications, we take the stiffened gas equation of state for the hydrodynamic energy

$$\varepsilon_s^h(\rho_s,\eta_s) = \frac{A_s \exp\left(\frac{\eta_s-\eta_{s0}}{c_{vs}}\right)\rho_s^{\gamma} + (\gamma_s-1)p_{\infty s}}{(\gamma_s-1)\rho_s}, \tag{10}$$

and for the elastic energy

$$\varepsilon_s^e(\widetilde{G},\eta_s) = \frac{\mu_s}{4\rho_{s0}} tr((\widetilde{G}-I)^2). \tag{11}$$

Here, $A_s, \eta_{s0}, p_{\infty s}, \gamma_s > 1, c_{vs}$ and $\mu_s$ are constants. The shear modulus $\mu_s$ may also depend on the entropy. In the following we consider the case where $\mu_s$ is a material constant. In the limit of small deformations the Hooke law is recovered. In the limit of large deformations, the solid behaves as a fluid. This equation of state is suitable for the treatment of shocks of large amplitude. In particular, the corresponding stress tensor in a solid is:

$$\sigma_s = -p_s I + \hat{\sigma}_s, \quad \hat{\sigma}_s = -\mu_s \frac{\rho_s}{\rho_{s0}}\left(\frac{1}{|G|^{2/3}}\left(G^2 - \frac{J_2}{3}I\right) - \frac{1}{|G|^{1/3}}\left(G - \frac{J_1}{3}I\right)\right), \quad tr(\hat{\sigma}_s) = 0. \tag{12}$$

An important question is whether the governing equations are hyperbolic. We refer to Godunov and Romenskii [17] for a general criterion of hyperbolicity of equations of hyperelasticity with geometric constraint (4). It can be shown that with the equations of state (10) and (11), the one-dimensional equations of motion are hyperbolic in a full domain of variables.[1]

In this article, we will use the symmetrization approach to prove the hyperbolicity of a one-dimensional multiphase model derived for numerical modelling of interfaces.

### 2.2. Euler equations of compressible fluids

When the shear modulus $\mu_s$ is zero, we recover the Euler equations of compressible fluids (we use the index $g$ for unknowns, the velocity $\mathbf{v}$ is without index):

$$\frac{\partial \rho_g}{\partial t} + \mathrm{div}(\rho_g \mathbf{v}) = 0, \tag{13a}$$

$$\frac{\partial \rho_g \mathbf{v}}{\partial t} + \mathrm{div}(\rho_g \mathbf{v}\otimes\mathbf{v} - \sigma_g) = 0, \tag{13b}$$

$$\frac{\partial}{\partial t}\left(\rho_g\left(e_g + \frac{\mathbf{v}\cdot\mathbf{v}}{2}\right)\right) + \mathrm{div}\left(\rho_g \mathbf{v}\left(e_g + \frac{\mathbf{v}\cdot\mathbf{v}}{2}\right) - \sigma_g\mathbf{v}\right) = 0, \tag{13c}$$

with the corresponding Gibbs identity

$$\theta_g d\eta_g = de_g + p_g d\left(\frac{1}{\rho_g}\right). \tag{14}$$

Here, $\eta_g$ is the entropy, $\theta_g$ is the temperature, $\rho_g$ is the density, $e_g = \varepsilon_g^h(\rho_g,\eta_g)$ is the specific energy of the gas, $\sigma_g = -p_g I$ is the stress tensor, $p_g$ is the pressure, $I$ is the identity tensor. Eq. (13c) are the Euler–Lagrange equations for the Lagrangian

$$L_g = \int_{\Omega_t} \rho_g\left(\frac{\mathbf{v}\cdot\mathbf{v}}{2} - \varepsilon_g^h\left(\rho_g,\eta_g\right)\right)d\Omega,$$

where the mass and entropy conservation laws should be considered as constraints [32]. The equations are hyperbolic if the internal energy $\varepsilon_g^h$ is a convex function of $\tau_g = 1/\rho_g$ and $\eta_g$ [16,17].

[1] In Gavrilyuk et al. [14] typos are present in the characteristic polynomial calculated for the two-dimensional case (see formula (36) in that paper). It should be written as $(u-v)^4 + (u-v)^2(a^{(1)}\sigma_{11,1} + a^{(2)}\sigma_{11,2} + \sigma_{12,2})/\rho + a^{(1)}(\sigma_{11,1}\sigma_{12,2} - \sigma_{12,1}\sigma_{11,2})/\rho^2 = 0$. Here $u$ is the $x$-component of the velocity, $v$ is the eigenvalue, $a^{(1)}, a^{(2)}$ are the $x$- components of the vectors $\mathbf{e}^1$ and $\mathbf{e}^2$, and the density $\rho$ is the density of a solid. The notation $\sigma_{ij,\alpha}$ means the derivative of the stress component $\sigma_{ij}$ with respect to $a^{(\alpha)}$.

## 3. Solid–fluid compressible mixtures

The diffuse interface model for solid–fluid coupling is based on an "averaged" formulation able to describe the dynamics of pure components (solid and fluid), as well as the interaction at the interface between components. It is necessary that in the limit of vanishing volume fractions the model gives the governing equations of pure phases (7) and (8) and (13) and (14). The difficulty in writing such a model is that the number of equations describing pure phases is not the same in different phases, so the direct application of a classical averaging technique based on averaging the same number of conservation laws is questionable. The relations on contact discontinuity in pure phases are also different: for a solid, the sliding is forbidden while for the gas it is not. We want to derive such a model permitting to account for the sliding on the solid–gas interfaces. We also want to formulate a simplified one-velocity model describing interaction on a gas–solid interface. First, the averaged mass conservation laws should be postulated:

$$\frac{\partial(\alpha_s\rho_s)}{\partial t} + \operatorname{div}(\alpha_s\rho_s\mathbf{v}) = 0, \tag{15}$$

$$\frac{\partial(\alpha_g\rho_g)}{\partial t} + \operatorname{div}(\alpha_g\rho_g\mathbf{v}) = 0. \tag{16}$$

Here, $\alpha_s + \alpha_g = 1$, $\alpha_s$ and $\alpha_g$ are the volume fractions of components, and $\mathbf{v}$ is the average velocity. However, the mass conservation law for a solid component is not sufficient. The equations for the local cobasis should also be written in "averaged" form. The equations for $\mathbf{e}^\beta$ should satisfy the following restrictions. First, the mass conservation law (15) should be a consequence of these equations. Second, for irreversible process the equations should be compatible with the entropy inequality.

Usually, direct averaging methods [5,6,15,33]) or variational approaches [13,31] are used for such "averaging" modeling. Another method (DEM – Discrete Equations Method) was recently developed in Abgrall and Saurel [3], Saurel et al. [31] and Chinnayya et al. [7]. The present developments are based on the variational approach.

### 3.1. Geometric equations and the mass conservation law

Let us rewrite the mass conservation law (15) in the Lagrangian coordinates $\mathbf{X} = \{X^\alpha\}$:

$$\rho_s = \rho_{s0}|G|^{1/2}, \tag{17}$$

where $\rho_{s0}(\mathbf{X})$ is a solid reference density. Multiplying it by $\alpha_s$ we obtain

$$\alpha_s\rho_s = \alpha_s\rho_{s0}|G|^{1/2}.$$

Since $G = \sum_{\beta=1}^{3}\mathbf{e}^\beta \otimes \mathbf{e}^\beta$, it can also be rewritten in the form

$$\alpha_s\rho_s = \rho_{s0}|\langle G\rangle|^{1/2},$$

where we have introduced the averaged tensor $\langle G\rangle$ defined as:

$$\langle G\rangle = \sum_{\beta=1}^{3}\alpha_s^{n_\beta}\mathbf{e}^\beta \otimes \alpha_s^{n_\beta}\mathbf{e}^\beta,$$

where the vectors $\alpha_s^{n_\beta}\mathbf{e}^\beta$ verify equations

$$\frac{\partial(\alpha_s^{n_\beta}\mathbf{e}^\beta)}{\partial t} + \mathbf{V}(\alpha_s^{n_\beta}\mathbf{e}^\beta \cdot \mathbf{v}) = 0, \tag{18}$$

$$\operatorname{rot}(\alpha_s^{n_\beta}\mathbf{e}^\beta) = 0. \tag{19}$$

and the numbers $n_\beta$ are such that

$$n_\beta > 0, \quad \sum_{\beta=1}^{3} n_\beta = 1.$$

Relations (18) and (19) allow to say that $\langle G\rangle$ is the averaged Finger tensor:

$$\langle G\rangle = \langle F^T\rangle^{-1}\langle F\rangle^{-1},$$

where $\langle F\rangle$ is the averaged deformation gradient. In pure solid phase ($\alpha_s = 1$) or in a homogeneous case ($\alpha_s = const$) we find usual geometric equations (3) and (4). The numbers $n_\beta$ characterize the mixture anisotropy. The Eqs. (18) and (19) can be seen as the averages of Eqs. (3) and (4) along "nearly one-dimensional" directions. For isotropic case, we have to take

$$n_1 = n_2 = n_3 = \frac{1}{3}. \tag{20}$$

For applications, we will consider only the isotropic case (20).

Eqs. (18) and (19) imply the following non-conservative geometric equation:

$$\frac{\partial \mathbf{E}^\beta}{\partial t} + \nabla(\mathbf{E}^\beta \cdot \mathbf{v}) = -\mathrm{rot}\mathbf{E}^\beta \wedge \mathbf{v}, \tag{21}$$

Here, we introduce a modified cobasis vectors:

$$\mathbf{E}^\beta = \alpha_s^{1/3}\mathbf{e}^\beta. \tag{22}$$

In particular, this equation also implies that if

$$\mathrm{rot}\mathbf{E}^\beta = 0,$$

at $t = 0$, it vanishes at all times. Eq. (21) is the analog of the nonconservative Eq. (5) of conventional elasticity. The averaged non-conservative equations (21) and (22) are compatible with the solid mass balance equation. To prove that, we rewrite it in a non-conservative form:

$$\frac{D\mathbf{e}^\beta}{Dt} + \left(\frac{\partial \mathbf{v}}{\partial \mathbf{x}}\right)^T \mathbf{e}^\beta + \frac{1}{3}\mathbf{e}^\beta \alpha_s^{-1}\frac{D\alpha_s}{Dt} = 0. \tag{23}$$

Calculating the material derivative of $G$ defined by (1) we obtain by using (23):

$$\begin{aligned}\frac{DG}{Dt} &= \sum_{\beta=1}^{3}\left(\frac{D\mathbf{e}^\beta}{Dt}\otimes\mathbf{e}^\beta + \mathbf{e}^\beta\otimes\frac{D\mathbf{e}^\beta}{Dt}\right) = \sum_{\beta=1}^{3}\left(\left(-\left(\frac{\partial \mathbf{v}}{\partial \mathbf{x}}\right)^T\mathbf{e}^\beta + \frac{1}{3}\mathbf{e}^\beta\alpha_s^{-1}\frac{D\alpha_s}{Dt}\right)\otimes\mathbf{e}^\beta + \mathbf{e}^\beta\otimes\left(-\left(\frac{\partial \mathbf{v}}{\partial \mathbf{x}}\right)^T\mathbf{e}^\beta + \frac{1}{3}\mathbf{e}^\beta\alpha_s^{-1}\frac{D\alpha_s}{Dt}\right)\right)\\ &= -\left(\frac{\partial \mathbf{v}}{\partial \mathbf{x}}\right)^T G - G\left(\frac{\partial \mathbf{v}}{\partial \mathbf{x}}\right) - \frac{2}{3}\alpha_s^{-1}\frac{D\alpha_s}{Dt}G.\end{aligned}$$

The evolution equation for $G$ is then

$$\frac{DG}{Dt} + \left(\frac{\partial \mathbf{v}}{\partial \mathbf{x}}\right)^T G + G\left(\frac{\partial \mathbf{v}}{\partial \mathbf{x}}\right) = -\frac{2}{3}\alpha_s^{-1}\frac{D\alpha_s}{Dt}G. \tag{24}$$

Eq. (24) can be rewritten in terms of $\langle G\rangle = \sum_{\beta=1}^{3}\mathbf{E}^\beta\otimes\mathbf{E}^\beta$:

$$\frac{D\langle G\rangle}{Dt} + \left(\frac{\partial \mathbf{v}}{\partial \mathbf{x}}\right)^T\langle G\rangle + \langle G\rangle\left(\frac{\partial \mathbf{v}}{\partial \mathbf{x}}\right) = 0.$$

Differentiating the Eq. (17) along trajectories and using (24) we obtain:

$$\begin{aligned}\frac{D\rho_s}{Dt} &= \frac{\rho_{s0}}{2|G|^{1/2}}tr\left(\frac{\partial|G|}{\partial G}\frac{DG}{Dt}\right) = \frac{\rho_{s0}|G|^{1/2}}{2}tr\left(G^{-1}\frac{DG}{Dt}\right) = \frac{\rho_{s0}|G|^{1/2}}{2}tr\left(G^{-1}\left(-\left(\frac{\partial \mathbf{v}}{\partial \mathbf{x}}\right)^T G - G\left(\frac{\partial \mathbf{v}}{\partial \mathbf{x}}\right) - \frac{2}{3}\alpha_s^{-1}\frac{D\alpha_s}{Dt}G\right)\right)\\ &= -\rho_s\mathrm{div}(\mathbf{v}) - \rho_s\alpha_s^{-1}\frac{D\alpha_s}{Dt}.\end{aligned}$$

Or

$$\alpha_s\frac{D\rho_s}{Dt} + \rho_s\frac{D\alpha_s}{Dt} + \alpha_s\rho_s\mathrm{div}(\mathbf{v}) = 0.$$

This is exactly a non-conservative form of the mass conservation law for the solid phase (15).

### 3.2. Reversible equilibrium model

To derive a reversible model, we will use the Hamilton principle of stationary action (see the basic definitions in Serrin [32]). Consider the Lagrangian:

$$L = \int_{\Omega_t}\rho\left(\frac{\mathbf{v}\cdot\mathbf{v}}{2} - e\right)d\Omega$$

where

$$\rho = \alpha_s\rho_s + \alpha_g\rho_g, \quad \rho e = \alpha_s\rho_s e_s + \alpha_g\rho_g e_g.$$

The derivation of the governing equations is analogous to that given, for example, in Gavrilyuk and Gouin [12] and Gavrilyuk and Saurel [13] for various models of continuum mechanics. We recall the main ingredients of this approach. Consider a family of smooth virtual motions

$$\mathbf{x} = \mathbf{\Phi}(t, \mathbf{X}, \epsilon)$$

where $\epsilon$ is a small parameter in the vicinity of zero. The real motion corresponds to $\epsilon = 0 : \mathbf{\Phi}(t, \mathbf{X}, 0) = \boldsymbol{\phi}(t, \mathbf{X})$. The virtual displacement $\delta\mathbf{x}$ is defined as

$$\delta\mathbf{x} = \left.\frac{d}{d\epsilon}\right|_{\epsilon=0} \mathbf{\Phi}$$

The virtual displacements are chosen to vanish at the boundary of the domain $\Omega_t$ and at the instants $t_1$and $t_2$ between which the Hamilton action $a$ is considered:

$$a = \int_{t_1}^{t_2} L dt. \tag{25}$$

Also, the variation of the volume fraction $\delta\alpha_s$ will be considered as an independent one. The Hamilton principle says:

$$\delta a = 0,$$

for any $\delta\mathbf{x}$ vanishing at the boundary of $\Omega_t$ and at the instants $t_1$and $t_2$. The geometric equations, mass and entropy conservation equations of each phase are considered as differential constraints. The mass conservation laws can be also rewritten in terms of the mass concentrations $Y_s$ and $Y_g$:

$$\frac{DY_s}{Dt} = 0, \quad \frac{DY_g}{Dt} = 0, \quad Y_s = \frac{\alpha_s\rho_s}{\rho}, \quad Y_g = \frac{\alpha_g\rho_g}{\rho}, \quad Y_s + Y_g = 1.$$

To apply the Hamilton principle we find the variations of $\rho, \mathbf{v}, Y_s, Y_g, \eta_g, \eta_s$ and $\mathbf{E}^\beta = \alpha_s^{\frac{1}{3}}\mathbf{e}^\beta$ as functions of virtual displacements at fixed Lagrangian coordinates (these variations are called Lagrangian variations):

$$\delta\rho = -\rho\mathrm{div}(\delta\mathbf{x}), \quad \delta\mathbf{v} = \frac{\partial\delta\mathbf{x}}{\partial t}, \quad \delta\eta_i = 0, \quad \delta Y_i = 0, \tag{26}$$

$$\delta\mathbf{E}^\beta = -\left(\frac{\partial\delta\mathbf{x}}{\partial\mathbf{x}}\right)^T \mathbf{E}^\beta.$$

Here, and below the symbol $\delta$ always means the variation at fixed Lagrangian coordinates. The first formula comes from the mixture mass conservation law written in Lagrangian coordinates:

$$\rho(t, \mathbf{X})\left|\frac{\partial\boldsymbol{\phi}(t, \mathbf{X})}{\partial\mathbf{X}}\right| = \rho_0(\mathbf{X}),$$

where $\rho_0(\mathbf{X})$ is the averaged reference density. Writing it for the virtual motion

$$\rho(t, \mathbf{X}, \epsilon)\left|\frac{\partial\mathbf{\Phi}(t, \mathbf{X}, \epsilon)}{\partial\mathbf{X}}\right| = \rho_0(\mathbf{X}),$$

and deriving it with respect to $\epsilon$ we obtain the formula for the variation of $\rho$. The formulas for the variation of the velocity, the entropy and the mass fraction are direct. This derivation can be found in Serrin [32] (see also [12,13]). The last formula giving the variation of $\mathbf{E}^\beta$ is a consequence of the fact that the Eqs. (18) and (19) are equivalent to the following ones: there exist a potential $\Phi^\beta$ such that

$$\frac{D\Phi^\beta}{Dt} = 0,$$

$$\nabla\Phi^\beta = \alpha_s^{\frac{1}{3}}\mathbf{e}^\beta = \mathbf{E}^\beta.$$

It follows from the definition of $\Phi^\beta$ that its Lagrangian variation is zero:

$$\delta\Phi^\beta = 0.$$

Here, we abuse the notations by using the same symbol $\Phi^\beta$ for unknowns which are considered both in the Eulerian and the Lagrangian coordinates. Since

$$\delta F^{-1} = -F^{-1}\delta F F^{-1} = -F^{-1}\frac{\partial\delta\mathbf{x}}{\partial\mathbf{X}}F^{-1} = -F^{-1}\frac{\partial\delta\mathbf{x}}{\partial\mathbf{x}}$$

we get from the definition of $\mathbf{E}^\beta$:

$$\delta\mathbf{E}^\beta = \delta\nabla\Phi^\beta = \delta(F^{-T}\nabla_{\mathbf{X}}\Phi^\beta) = -\left(F^{-1}\frac{\partial\delta\mathbf{x}}{\partial\mathbf{x}}\right)^T\nabla_{\mathbf{X}}\Phi^\beta = -\left(\frac{\partial\delta\mathbf{x}}{\partial\mathbf{x}}\right)^T F^{-T}\nabla_{\mathbf{X}}\Phi^\beta = -\left(\frac{\partial\delta\mathbf{x}}{\partial\mathbf{x}}\right)^T\mathbf{E}^\beta.$$

In particular, the variation of $\langle G\rangle = \alpha_s^{\frac{2}{3}} G$ is given by:

$$\delta\langle G\rangle = \delta\left(\alpha_s^{\frac{2}{3}} G\right) = \delta\left(\sum_{\beta=1}^{3} \mathbf{E}^\beta \otimes \mathbf{E}^\beta\right) = -\left(\frac{\partial \delta\mathbf{x}}{\partial \mathbf{x}}\right)^T \langle G\rangle - \langle G\rangle \left(\frac{\partial \delta\mathbf{x}}{\partial \mathbf{x}}\right). \tag{27}$$

The Gibbs identity for the internal energy of a solid phase is

$$\begin{aligned} de_s &= tr\left(\frac{\partial e_s}{\partial G} dG\right) + \theta_s d\eta_s = -\frac{1}{2\rho_s} tr\left(\sigma_s (\alpha_s^{2/3} G)^{-1} d(\alpha_s^{2/3} G) - \frac{2}{3}\sigma_s \alpha_s^{-1} d(\alpha_s)\right) + \theta_s d\eta_s \\ &= -\frac{1}{2\rho_s} tr\left(\sigma_s (\alpha_s^{2/3} G)^{-1} d(\alpha_s^{2/3} G)\right) + \theta_s d\eta_s - \frac{p_s}{\alpha_s \rho_s} d\alpha_s = -\frac{1}{2\rho_s} tr(\sigma_s \langle G\rangle^{-1} d\langle G\rangle) + \theta_s d\eta_s - \frac{p_s}{\alpha_s \rho_s} d\alpha_s. \end{aligned}$$

Then (27) implies:

$$\delta e_s = -\frac{1}{\rho_s} tr\left(\sigma_s \frac{\partial \delta\mathbf{x}}{\partial \mathbf{x}}\right) + \theta_s \delta\eta_s - \frac{p_s}{\alpha_s \rho_s} \delta\alpha_s. \tag{28}$$

Analogous considerations give a simpler variation for the gas phase:

$$\delta e_g = -\frac{1}{\rho_g} tr\left(\sigma_g \frac{\partial \delta\mathbf{x}}{\partial \mathbf{x}}\right) + \theta_g \delta\eta_g - \frac{p_g}{\alpha_g \rho_g} \delta\alpha_s = \frac{p_g}{\rho_g} \operatorname{div} \delta\mathbf{x} + \theta_g \delta\eta_g - \frac{p_g}{\alpha_g \rho_g} \delta\alpha_g. \tag{29}$$

Now, we are ready to take the variation of the Hamilton action (25). We use formulas (26), (28), (29) and the mass conservation law: $\rho d\Omega = \rho_0(\mathbf{X}) d\Omega_0$ to present the variation of $a$ in the form:

$$\begin{aligned} 0 = \delta a &= \delta \int_{t_1}^{t_2} \int_{\Omega_t} \rho\left(\frac{\mathbf{v}\cdot\mathbf{v}}{2} - e\right) d\Omega dt = \delta \int_{t_1}^{t_2} \int_{\Omega_0} \rho_0(\mathbf{X})\left(\frac{\mathbf{v}\cdot\mathbf{v}}{2} - e\right) d\Omega_0 dt = \int_{t_1}^{t_2} \int_{\Omega_0} \rho_0(\mathbf{X})(\delta\mathbf{v}\cdot\mathbf{v} - \delta e) d\Omega_0 dt \\ &= \int_{t_1}^{t_2} \int_{\Omega_0} \rho_0(\mathbf{X}) \left(\frac{\partial \delta\mathbf{x}}{\partial t}\cdot\mathbf{v} + Y_s\left(\frac{1}{\rho_s} tr\left(\sigma_s \frac{\partial \delta\mathbf{x}}{\partial \mathbf{x}}\right) + \frac{p_s}{\alpha_s \rho_s}\delta\alpha_s\right) - Y_g\left(\frac{p_g}{\rho_g} \operatorname{div}\delta\mathbf{x} - \frac{p_g}{\alpha_g \rho_g}\delta\alpha_g\right)\right) d\Omega_0 dt \\ &= \int_{t_1}^{t_2} \int_{\Omega_0} \rho_0(\mathbf{X}) \left(\frac{\partial \delta\mathbf{x}}{\partial t}\cdot\mathbf{v} + \frac{1}{\rho}\left(tr\left((\alpha_s\sigma_s - \alpha_g p_g)\frac{\partial \delta\mathbf{x}}{\partial \mathbf{x}}\right) + p_s\delta\alpha_s + p_g\delta\alpha_g\right)\right) d\Omega_0 dt. \end{aligned}$$

Since $\delta\alpha_s + \delta\alpha_g = 0$, it implies the equilibrium condition:

$$p_s - p_g = 0. \tag{30}$$

Here,

$$p_s = -\frac{1}{3} tr(\sigma_s), \quad p_g = -\frac{1}{3} tr(\sigma_g).$$

Turning back to the Eulerian coordinates we transform the last variation to the following one:

$$0 = \delta a = \int_{t_1}^{t_2} \int_{\Omega_t} \left(\frac{D\delta\mathbf{x}}{Dt}\cdot \rho\mathbf{v} + tr\left((\alpha_s\sigma_s - \alpha_g p_g)\frac{\partial \delta\mathbf{x}}{\partial \mathbf{x}}\right)\right) d\Omega_t dt$$

Integrating by parts and taking into account the fact that $\delta\mathbf{x}$ is vanishing at the boundary $\Omega_t \times [t_1, t_2]$ we obtain

$$0 = \delta a = -\int_{t_1}^{t_2} \int_{\Omega_t} \left(\frac{\partial \rho\mathbf{v}}{\partial t} + \operatorname{div}(\rho\mathbf{v}\otimes\mathbf{v} - (\alpha_s\sigma_s + \alpha_g\sigma_g))\right)\cdot \delta\mathbf{x} d\Omega dt$$

for any $\delta\mathbf{x}$ vanishing at the boundary $\Omega_t \times [t_1, t_2]$. It implies the momentum equation:

$$\frac{\partial \rho\mathbf{v}}{\partial t} + \operatorname{div}(\rho\mathbf{v}\otimes\mathbf{v} - (\alpha_s\sigma_s + \alpha_g\sigma_g)) = 0. \tag{31}$$

The stress tensor $\sigma_s$ in a solid phase is defined by (8), the stress tensor in the gas phase is $\sigma_g = -p_g I$. Since the energy equation for the solid component is written in separate form (9), the solid pressure is determined only by its hydrodynamic part:

$$p_s = \rho_s^2 \frac{\partial \varepsilon_s^h(\rho_s, \eta_s)}{\partial \rho_s}.$$

The gas pressure is determined as:

$$p_g = \rho_g^2 \frac{\partial \varepsilon_g^h(\rho_g, \eta_g)}{\partial \rho_g}.$$

The entropy conservation equations

$$\frac{D\eta_s}{Dt} = 0, \quad \frac{D\eta_g}{Dt} = 0,$$

complemented by the mass and momentum balance laws imply the mixture energy conservation law:

$$\frac{\partial}{\partial t}\left(\rho\left(e+\frac{\mathbf{v}\cdot\mathbf{v}}{2}\right)\right)+\operatorname{div}\left(\rho\mathbf{v}\left(e+\frac{\mathbf{v}\cdot\mathbf{v}}{2}\right)-(\alpha_s\sigma_s+\alpha_g\sigma_g)\mathbf{v}\right)=0. \tag{32}$$

Finally, the equilibrium solid–gas governing equations are

$$\frac{\partial \mathbf{E}^\beta}{\partial t}+\nabla(\mathbf{E}^\beta\cdot\mathbf{v})=-\operatorname{rot}\mathbf{E}^\beta\wedge\mathbf{v}, \tag{33a}$$

$$\operatorname{rot}\mathbf{E}^\beta=0, \tag{33b}$$

$$\frac{\partial(\alpha_g\rho_g)}{\partial t}+\operatorname{div}(\alpha_g\rho_g\mathbf{v})=0, \tag{33c}$$

$$\frac{\partial\rho\mathbf{v}}{\partial t}+\operatorname{div}(\rho\mathbf{v}\otimes\mathbf{v}-(\alpha_s\sigma_s+\alpha_g\sigma_g))=0, \tag{33d}$$

$$\frac{D\eta_s}{Dt}=0,\quad \frac{D\eta_g}{Dt}=0, \tag{33e}$$

$$p_s=p_g. \tag{33f}$$

Eq. (33f) admit the energy conservation law (32).

Taking the material derivative of the relation $p_s=p_g$ representing the mechanical equilibrium between phases we obtain a non-conservative equation for the volume fraction which is analogous to that used in the case of fluid–fluid mixtures [20,25]:

$$\frac{D\alpha_s}{Dt}+K\operatorname{div}\mathbf{v}=0,\quad K=\frac{\rho_s c_s^2-\rho_g c_g^2}{\frac{\rho_g c_g^2}{\alpha_g}+\frac{\rho_s c_s^2}{\alpha_s}}. \tag{34}$$

### 3.3. Hyperbolicity of the equilibrium model

The equilibrium model (33f) is hyperbolic. Since we do not intend to use the equilibrium model for computations for the reasons explained below in this paragraph, we give the proof of hyperbolicity in the simplest case of one-dimensional longitudinal waves where $\mathbf{v}=(u,0,0)^T$. Also, the specific entropies $\eta_s,\eta_g$, the initial solid density $\rho_{s0}$ and the mass fractions $Y_g,Y_s$ are supposed to be constant: the equations for these variables give only contact characteristics. Let

$$\mathbf{E}^\beta=\begin{pmatrix}A^{(\beta)}\\ B^{(\beta)}\\ C^{(\beta)}\end{pmatrix},\quad \beta=1,2,3$$

Relation $\operatorname{rot}\mathbf{E}^\beta=0$ implies that only the components $A^{(\beta)}$ vary, the other components are constant. The vectors $\mathbf{E}^\beta$ can be chosen in such a way that initially they form an orthogonal basis. If only longitudinal waves are considered, we can always suppose that $B^{(1)}=C^{(1)}=0, A^{(2)}=1, B^{(2)}=const, C^{(2)}=0, A^{(3)}=0, B^{(3)}=0, C^{(3)}=const$. The matrix $\langle G\rangle$ becomes:

$$\begin{aligned}\langle G\rangle&=\begin{pmatrix}(A^{(1)})^2+(A^{(2)})^2+(A^{(3)})^2 & A^{(1)}B^{(1)}+A^{(2)}B^{(2)}+A^{(3)}B^{(3)} & A^{(1)}C^{(1)}+A^{(2)}C^{(2)}+A^{(3)}C^{(3)}\\ A^{(1)}B^{(1)}+A^{(2)}B^{(2)}+A^{(3)}B^{(3)} & (B^{(1)})^2+(B^{(2)})^2+(B^{(3)})^2 & B^{(1)}C^{(1)}+B^{(2)}C^{(2)}+B^{(3)}C^{(3)}\\ A^{(1)}C^{(1)}+A^{(2)}C^{(2)}+A^{(3)}C^{(3)} & B^{(1)}C^{(1)}+B^{(2)}C^{(2)}+B^{(3)}C^{(3)} & (C^{(1)})^2+(C^{(2)})^2+(C^{(3)})^2\end{pmatrix}\\ &=\begin{pmatrix}(A^{(1)})^2 & 0 & 0\\ 0 & (B^{(2)})^2 & 0\\ 0 & 0 & (C^{(3)})^2\end{pmatrix}.\end{aligned}$$

To be compatible with the mass conservation law for a solid, we should initially have:

$$|\langle G\rangle|^{1/2}(0,\mathbf{X})=A^{(1)}B^{(2)}C^{(3)}=\alpha_{s0}(\mathbf{X}).$$

The hyperbolicity analysis which follows, does not depend on the choice of constants $B^{(2)}$ and $C^{(3)}$. For example, we can take $B^{(2)}=1, C^{(3)}=1$, then $A^{(1)}=\alpha_{s0}(\mathbf{X})$. The governing equations are:

$$\frac{\partial\rho}{\partial t}+\frac{\partial(\rho u)}{\partial x}=0,$$

$$\frac{\partial A^{(1)}}{\partial t}+\frac{\partial(A^{(1)}u)}{\partial x}=0,$$

$$\rho\left(\frac{\partial u}{\partial t}+u\frac{\partial u}{\partial x}\right)+\frac{\partial(p-\alpha_s\hat{\sigma}_{11s})}{\partial x}=0,$$

$$p=p_g=p_s.$$

The component $\alpha_s\hat{\sigma}_{11s}$of the deviatoric part of the averaged solid stress tensor $\alpha_s\hat{\sigma}_s$ in a particular case of the elastic energy given by (11) is (see (12)):

$$-\alpha_s\hat{\sigma}_{11s} = \frac{2}{3}\mu_s f(A^{(1)}),$$

where

$$f(A^{(1)}) = \frac{(A^{(1)})^4 - 1 - (A^{(1)})^{2/3}((A^{(1)})^2 - 1)}{(A^{(1)})^{1/3}}.$$

It has the following property:

$$f(1) = 0, \quad \frac{df}{dA^{(1)}} > 0, \quad \frac{df}{dA^{(1)}}(1) = 2.$$

The sound speed $c^2$ in this system is

$$c^2 = c_W^2 + \frac{2\mu_s}{3\rho}A^{(1)}\frac{df}{dA^{(1)}}.$$

where $c_W$ is the Wood sound speed defined by:

$$\frac{1}{\rho c_W^2} = \frac{\alpha_g}{\rho_g c_g^2} + \frac{\alpha_s}{\rho_s c_s^2},$$

where $c_g^2$ and $c_s^2$ are the hydrodynamical sound speeds:

$$c_i^2 = \frac{\partial p_i}{\partial \rho_i}\Big|_{\eta_i = const}, \quad i = s, g.$$

In the limit of small deformations the sound speed is

$$c^2 \approx c_W^2 + \frac{4\mu_s}{3\rho_0}.$$

The equilibrium model poses however serious computational challenges, those are even present in the context of two fluids i.e. where the solid stress tensor is assumed to be spherical and where the equations for $\mathbf{E}^\beta$ are omitted. In this fluid limit, the Kapila et al. [20] model is recovered. This model is composed of two mass equations, a mixture momentum equation and a mixture energy equation. These equations are in conservative form. The closure is achieved by the fulfilment of the pressure equilibrium condition resulting in a transport equation for the volume fraction (34) and containing a non-conservative term involving the velocity divergence and phase bulk moduli. This last equation poses serious computational challenges:

- Shock computations within the context of a non-conservative model.
- Volume fraction positivity, when dealing with shocks and strong expansion waves. The term involving a velocity divergence in the volume fraction evolution equation is particularly difficult to approximate [26]. This is particularly important for the dynamic appearance of interfaces in cavitating flows.

Also, the Wood sound speed, which is the sound speed in the fluid–fluid model, can be extremely low compared to the sound speeds of pure phases. As a consequence, it produces delay in wave transmission through numerical diffuse interfaces.

To circumvent these difficulties, in the context of fluid–fluid interfaces, a mechanical non-equilibrium model was promoted in Saurel et al. [30]. In this context, a three-step algorithm was proposed:

- A hyperbolic step with the multiphase flow model out of pressure equilibrium having a monotonic sound speed. The building of approximate Riemann solvers and Godunov type scheme insuring volume fraction positivity is an easy task.
- A stiff pressure relaxation step is used to restore the mechanical equilibrium condition.
- Reset of internal energies of components with the help of total energy conservation equation and mixture equations of state.

This procedure was shown asymptotically convergent to solutions of the mechanical equilibrium model of Kapila et al. [20]. The three-step algorithm was also demonstrated very robust, accurate and computationally efficient. We will follow the same strategy for the solid–fluid interfaces. In this aim, a solid–fluid mechanical non-equilibrium model is needed.

### 3.4. Non-equilibrium model

Since the local equilibrium condition (30), which is valid in each point of the diffuse fluid–solid interface, is reminiscent to that for fluid–fluid interfaces (see [25,30,31]), we can construct in the same way a non-equilibrium model which must satisfy

the entropy inequality. We repeat again that we need this non-equilibrium model for numerical reasons discussed previously.

The introduction of dissipative terms is always a phenomenological procedure which however should respect some basic principles: the energy conservation and the entropy inequality. A typical procedure for the building of a non-equilibrium model consists in the following. We introduce first the dissipation function to replace the equilibrium condition (30) by a relaxation equation. The dissipation function $\mathscr{D}$ is quadratic with respect to generalized velocities if we neglect usual viscosity terms depending on higher derivatives of unknowns. In our case this generalized velocity is $\dot{\alpha}_s = \frac{D\alpha_s}{Dt}$. So, we take the dissipation function in the form:

$$\mathscr{D} = \frac{1}{2\mu_0}\dot{\alpha}_s^2,$$

where $\mu_0$ is a positive constant. The relaxation equation will be:

$$p_s - p_g = \frac{\partial \mathscr{D}}{\partial \dot{\alpha}_s} = \frac{\dot{\alpha}_s}{\mu_0}.$$

Now, we postulate the mixture energy equation. Since we neglect usual viscosity terms, it has the same form as (32):

$$\frac{\partial}{\partial t}\left(\rho\left(e + \frac{\mathbf{v}\cdot\mathbf{v}}{2}\right)\right) + \mathrm{div}\left(\rho\mathbf{v}\left(e + \frac{\mathbf{v}\cdot\mathbf{v}}{2}\right) - (\alpha_s\sigma_s + \alpha_g\sigma_g)\mathbf{v}\right) = 0. \tag{35}$$

Using (24), we can transform the energy Eq. (35) to the following one:

$$\alpha_s\rho_s\theta_s\frac{D\eta_s}{Dt} + \alpha_g\rho_g\theta_g\frac{D\eta_g}{Dt} = (p_s - p_g)\dot{\alpha}_s. \tag{36}$$

Indeed,

$$\begin{aligned}
0 &= \frac{\partial}{\partial t}\left(\rho\left(e + \frac{\mathbf{v}\cdot\mathbf{v}}{2}\right)\right) + \mathrm{div}\left(\rho\mathbf{v}\left(e + \frac{\mathbf{v}\cdot\mathbf{v}}{2}\right) - (\alpha_s\sigma_s + \alpha_g\sigma_g)\mathbf{v}\right)\\
&= \rho\frac{De}{Dt} - tr\left((\alpha_s\sigma_s + \alpha_g\sigma_g)\frac{\partial \mathbf{v}}{\partial \mathbf{x}}\right) = \rho\left(Y_s tr\left(\frac{\partial e_s}{\partial G}\frac{DG}{Dt}\right) + Y_s\frac{\partial e_s}{\partial \eta_s}\frac{D\eta_s}{Dt} + Y_g\frac{\partial e_g}{\partial \rho_g}\frac{D\rho_g}{Dt} + Y_g\frac{\partial e_g}{\partial \eta_g}\frac{D\eta_g}{Dt}\right) - tr\left((\alpha_s\sigma_s - \alpha_g p_g I)\frac{\partial \mathbf{v}}{\partial \mathbf{x}}\right)\\
&= \rho Y_s tr\left(-\frac{\partial e_s}{\partial G}\left(G\frac{\partial \mathbf{v}}{\partial \mathbf{x}} + \left(\frac{\partial \mathbf{v}}{\partial \mathbf{x}}\right)^T G + \frac{2}{3}\alpha_s^{-1}\frac{D\alpha_s}{Dt}G\right)\right) + \rho Y_s\frac{\partial e_s}{\partial \eta_s}\frac{D\eta_s}{Dt} + \rho\left(Y_g\frac{\partial e_g}{\partial \rho_g}\frac{D\rho_g}{Dt} + Y_g\frac{\partial e_g}{\partial \eta_g}\frac{D\eta_g}{Dt}\right) - tr\left((\alpha_s\sigma_s - \alpha_g p_g I)\frac{\partial \mathbf{v}}{\partial \mathbf{x}}\right)\\
&= \rho\left(\frac{1}{\rho}\frac{D\alpha_s}{Dt}\frac{1}{3}tr\left(-2\rho_s\frac{\partial e_s}{\partial G}G\right) + Y_g\frac{\partial e_g}{\partial \rho_g}\frac{D\rho_g}{Dt} + Y_s\frac{\partial e_s}{\partial \eta_s}\frac{D\eta_s}{Dt} + Y_g\frac{\partial e_g}{\partial \eta_g}\frac{D\eta_g}{Dt}\right) + \alpha_g p_g \mathrm{div}\mathbf{v}\\
&= \frac{D\alpha_s}{Dt}\frac{1}{3}tr(\sigma_s) + \rho\left(Y_s\theta_s\frac{D\eta_s}{Dt} + Y_g\theta_g\frac{D\eta_g}{Dt}\right) + p_g\left(\frac{\alpha_g}{\rho_g}\frac{D\rho_g}{Dt} + \alpha_g\mathrm{div}\mathbf{v}\right)\\
&= -p_s\frac{D\alpha_s}{Dt} + \rho\left(Y_s\theta_s\frac{D\eta_s}{Dt} + Y_g\theta_g\frac{D\eta_g}{Dt}\right) + p_g\left(\frac{\alpha_g}{\rho_g}\frac{D\rho_g}{Dt} + \alpha_g\mathrm{div}\mathbf{v} + \frac{D\alpha_g}{Dt} - \frac{D\alpha_g}{Dt}\right)\\
&= \rho\left(Y_s\theta_s\frac{D\eta_s}{Dt} + Y_g\theta_g\frac{D\eta_g}{Dt}\right) - \frac{D\alpha_s}{Dt}p_s - p_g\frac{D\alpha_g}{Dt}\\
&= \rho\left(Y_s\theta_s\frac{D\eta_s}{Dt} + Y_g\theta_g\frac{D\eta_g}{Dt}\right) - (p_s - p_g)\frac{D\alpha_s}{Dt}.
\end{aligned}$$

The Eq. (36) should be separated into two equations, because we need the entropy evolution equation for each component. Such a separation is always *phenomenological*. There is only one constraint to be respected: the entropy inequality. We use here a proposition adapted for fluid–fluid interaction models in [25,30,31]:

$$\alpha_s\rho_s\theta_s\frac{D\eta_s}{Dt} = (p_s - p_I)\dot{\alpha}_s, \quad \alpha_g\rho_g\theta_g\frac{D\eta_g}{Dt} = (p_g - p_I)\dot{\alpha}_g, \quad \dot{\alpha}_g + \dot{\alpha}_s = 0.$$

Obviously, they are compatible with (36). Here, $p_I$ is the interfacial pressure. The interfacial pressure is supposed to be a linear combination of average pressures in each phase [15]:

$$p_I = \beta_g p_s + \beta_s p_g, \quad \beta_s > 0, \quad \beta_g > 0, \quad \beta_s + \beta_g = 1.$$

In [31] the pressure $p_I$ was estimated as the pressure obtained from the solution of the linearized Riemann problem for which the left and right states have pressures $p_g$ and $p_s$ and equal velocities (see equation (34) in that paper for the entropies in the limit of equal velocities). It gives:

$$\beta_g = \frac{Z_g}{Z_g + Z_s}, \quad \beta_s = \frac{Z_s}{Z_g + Z_s},$$

where $Z_k = \rho_k c_k, k = s, g$ are acoustical impedances. Let us check that these hypotheses are compatible with the entropy inequality:

$$\frac{\partial(\rho\eta)}{\partial t} + \mathrm{div}(\rho\eta\mathbf{v}) \geqslant 0,$$

where $\eta$ is the mixture entropy:

$$\eta = Y_s\eta_s + Y_g\eta_g.$$

Indeed,

$$\begin{aligned}\frac{\partial(\rho\eta)}{\partial t} + \mathrm{div}(\rho\eta\mathbf{v}) &= \rho\frac{D\eta}{Dt} = \rho\frac{D(Y_s\eta_s + Y_g\eta_g)}{Dt} = \frac{1}{\theta_s}(p_s - p_I)\frac{D\alpha_s}{Dt} + \frac{1}{\theta_g}(p_g - p_I)\frac{D\alpha_g}{Dt}\\ &= \frac{\beta_g}{\theta_s}(p_s - p_g)\frac{D\alpha_s}{Dt} + \frac{\beta_s}{\theta_g}(p_g - p_s)\frac{D\alpha_g}{Dt} = \left(\frac{\beta_s}{\theta_g} + \frac{\beta_g}{\theta_s}\right)\frac{D\alpha_g}{Dt}(p_g - p_s) = \mu_0\left(\frac{\beta_s}{\theta_g} + \frac{\beta_g}{\theta_s}\right)(p_g - p_s)^2 \geqslant 0. \end{aligned} \tag{37}$$

Finally, the non-equilibrium model is

$$\frac{\partial(\mathbf{E}^\beta)}{\partial t} + \nabla(\mathbf{E}^\beta\cdot\mathbf{v}) = -\mathrm{rot}\mathbf{E}^\beta\wedge\mathbf{v}, \tag{38a}$$

$$\frac{\partial(\alpha_g\rho_g)}{\partial t} + \mathrm{div}(\alpha_g\rho_g\mathbf{v}) = 0, \tag{38b}$$

$$\frac{\partial\rho\mathbf{v}}{\partial t} + \mathrm{div}(\rho\mathbf{v}\otimes\mathbf{v} - (\alpha_s\sigma_s + \alpha_g\sigma_g)) = 0, \tag{38c}$$

$$\alpha_s\rho_s\theta_s\frac{D\eta_s}{Dt} = (p_s - p_I)\dot\alpha_s, \quad \alpha_g\rho_g\theta_g\frac{D\eta_g}{Dt} = (p_g - p_I)\dot\alpha_g, \quad \dot\alpha_g + \dot\alpha_s = 0, \tag{38d}$$

$$\frac{D\alpha_g}{Dt} = \dot\alpha_g = \mu_0(p_g - p_s), \quad \mu_0 > 0. \tag{38e}$$

The geometric equations (38a) and the entropy equations (38d) can also be rewritten in different forms which are more convenient for numerical computations:

$$\frac{\partial\mathbf{E}^\beta}{\partial t} + \frac{\partial\mathbf{E}^\beta}{\partial\mathbf{x}}\mathbf{v} + \left(\frac{\partial\mathbf{v}}{\partial\mathbf{x}}\right)^T\mathbf{E}^\beta = 0, \tag{39a}$$

$$\frac{\partial}{\partial t}(\alpha_s\rho_s e_s) + \mathrm{div}(\alpha_s\rho_s e_s\mathbf{v}) - \alpha_s tr\left(\sigma_s\frac{\partial\mathbf{v}}{\partial\mathbf{x}}\right) = -p_I\mu_0(p_s - p_g), \tag{39b}$$

$$\frac{\partial}{\partial t}(\alpha_g\rho_g e_g) + \mathrm{div}(\alpha_g\rho_g e_g\mathbf{v}) - \alpha_g tr\left(\sigma_g\frac{\partial\mathbf{v}}{\partial\mathbf{x}}\right) = -p_I\mu_0(p_g - p_s). \tag{39c}$$

The derivation of the first equation is direct, the last two equations appear indirectly in the derivation of the entropy inequality (37) (see also [30] in the case of fluid–fluid models).

### 3.5. Hyperbolicity of the non-equilibrium model

We have to be sure that the non-equilibrium model (38e) is hyperbolic. As in the equilibrium case, we can always suppose that the initial solid density $\rho_{s0}$ is constant. The governing equations for conservative variables $(\rho, \rho Y_g, \mathbf{E}^\beta, \rho\mathbf{v}, \rho\alpha_g, \rho\eta_s, \rho\eta_g)^T$ are:

$$\begin{aligned}&\frac{\partial\rho}{\partial t} + \mathrm{div}(\rho\mathbf{v}) = 0,\\ &\frac{\partial\rho Y_g}{\partial t} + \mathrm{div}(\rho Y_g\mathbf{v}) = 0,\\ &\frac{\partial\mathbf{E}^\beta}{\partial t} + \nabla(\mathbf{E}^\beta\cdot\mathbf{v}) = 0, \quad \mathrm{rot}\mathbf{E}^\beta = 0,\\ &\frac{\partial\rho\mathbf{v}}{\partial t} + \mathrm{div}(\rho\mathbf{v}\otimes\mathbf{v} - (\alpha_s\sigma_s + \alpha_g\sigma_g)) = 0,\\ &\frac{\partial\alpha_g\rho}{\partial t} + \mathrm{div}(\alpha_g\rho\mathbf{v}) = \rho\dot\alpha_g = \rho\mu_0(p_g - p_s), \quad \mu_0 > 0,\\ &\frac{\partial(\rho\eta_s)}{\partial t} + \mathrm{div}(\rho\eta_s\mathbf{v}) = \frac{(p_s - p_I)\dot\alpha_s}{Y_s\theta_s}, \quad \frac{\partial(\rho\eta_g)}{\partial t} + \mathrm{div}(\rho\eta_g\mathbf{v}) = \frac{(p_g - p_I)\dot\alpha_g}{Y_g\theta_g}, \quad \dot\alpha_g + \dot\alpha_s = 0.\end{aligned}$$

These equations admit the energy conservation law

$$\frac{\partial}{\partial t}\left(\rho\left(e + \frac{\mathbf{v}\cdot\mathbf{v}}{2}\right)\right) + \mathrm{div}\left(\rho\mathbf{v}\left(e + \frac{\mathbf{v}\cdot\mathbf{v}}{2}\right) - (\alpha_s\sigma_s + \alpha_g\sigma_g)\mathbf{v}\right) = 0,$$

where

$$e = Y_g e_g\left(\frac{Y_g\rho}{\alpha_g}, \frac{\rho\eta_g}{\rho}\right) + Y_s\left(\varepsilon_s^h\left(\frac{Y_s\rho}{\alpha_s}, \frac{\rho\eta_s}{\rho}\right) + \varepsilon_s^e\left(\frac{\langle G\rangle}{|\langle G\rangle|^{1/3}}\right)\right), \quad \langle G\rangle = \sum_{\beta=1}^{3} \mathbf{E}^\beta \otimes \mathbf{E}^\beta.$$

For the equation of state given by (11) the stress tensor is

$$\sigma_s = -p_s I - \mu_s \frac{\rho_s}{\rho_{s0}}\left(\frac{1}{|\langle G\rangle|^{2/3}}\left(\langle G\rangle^2 - \frac{\langle J_2\rangle}{3} I\right) - \frac{1}{|\langle G\rangle|^{1/3}}\left(\langle G\rangle - \frac{\langle J_1\rangle}{3} I\right)\right).$$

We present the proof of hyperbolicity in the one-dimensional case but in presence of shear waves. We denote $\mathbf{v} = (u, v, w)^T$. Relation rot$\mathbf{E}^\beta = 0$ implies that only components $A^{(\beta)}$ vary, the other components are constant. We can always suppose that initially the vectors $\mathbf{E}^\beta$coincide with the Cartesian basis. Hence, $B^{(2)} = C^{(3)} = 1, B^{(1)} = B^{(3)} = C^{(1)} = C^{(2)} = 0$. The matrix $\langle G\rangle$ becomes:

$$\begin{aligned}\langle G\rangle &= \begin{pmatrix} (A^{(1)})^2 + (A^{(2)})^2 + (A^{(3)})^2 & A^{(1)}B^{(1)} + A^{(2)}B^{(2)} + A^{(3)}B^{(3)} & A^{(1)}C^{(1)} + A^{(2)}C^{(2)} + A^{(3)}C^{(3)} \\ A^{(1)}B^{(1)} + A^{(2)}B^{(2)} + A^{(3)}B^{(3)} & (B^{(1)})^2 + (B^{(2)})^2 + (B^{(3)})^2 & B^{(1)}C^{(1)} + B^{(2)}C^{(2)} + B^{(3)}C^{(3)} \\ A^{(1)}C^{(1)} + A^{(2)}C^{(2)} + A^{(3)}C^{(3)} & B^{(1)}C^{(1)} + B^{(2)}C^{(2)} + B^{(3)}C^{(3)} & (C^{(1)})^2 + (C^{(2)})^2 + (C^{(3)})^2 \end{pmatrix} \\ &= \begin{pmatrix} (A^{(1)})^2 + (A^{(2)})^2 + (A^{(3)})^2 & A^{(2)} & A^{(3)} \\ A^{(2)} & 1 & 0 \\ A^{(3)} & 0 & 1 \end{pmatrix}.\end{aligned}$$

Obviously,

$$\begin{aligned}&|\langle G\rangle| = (A^{(1)})^2, \\ &\langle J_1\rangle = tr(\langle G\rangle) = (A^{(1)})^2 + (A^{(2)})^2 + (A^{(3)})^2 + 2, \\ &\langle J_2\rangle = tr(\langle G\rangle^2) = ((A^{(1)})^2 + (A^{(2)})^2 + (A^{(3)})^2)^2 + 2((A^{(2)})^2 + (A^{(3)})^2) + 2.\end{aligned}$$

We remark that the invariants $\langle J_1\rangle$ and $\langle J_2\rangle$ depend only on $A^{(1)}$ and $Z = \sqrt{(A^{(2)})^2 + (A^{(3)})^2}$. The one-dimensional governing equations become:

$$\frac{\partial A^{(1)}}{\partial t} + \frac{\partial (A^{(1)}u)}{\partial x} = 0, \tag{40a}$$

$$\frac{\partial A^{(2)}}{\partial t} + \frac{\partial (A^{(1)}u + v)}{\partial x} = 0, \tag{40b}$$

$$\frac{\partial A^{(3)}}{\partial t} + \frac{\partial (A^{(1)}u + w)}{\partial x} = 0, \tag{40c}$$

$$\frac{\partial \rho}{\partial t} + \frac{\partial (\rho u)}{\partial x} = 0, \tag{40d}$$

$$\frac{\partial \rho Y_g}{\partial t} + \frac{\partial (\rho Y_g u)}{\partial x} = 0, \tag{40e}$$

$$\frac{\partial \rho u}{\partial t} + \frac{\partial (\rho u^2 - \alpha_s\sigma_{s11} - \alpha_g\sigma_{g11})}{\partial x} = 0, \tag{40f}$$

$$\frac{\partial \rho v}{\partial t} + \frac{\partial (\rho u v - \alpha_s\sigma_{s12} - \alpha_g\sigma_{g12})}{\partial x} = 0, \tag{40g}$$

$$\frac{\partial \rho w}{\partial t} + \frac{\partial (\rho u w - \alpha_s\sigma_{s13} - \alpha_g\sigma_{g13})}{\partial x} = 0, \tag{40h}$$

$$\frac{\partial \rho\alpha_g}{\partial t} + \frac{\partial (\rho\alpha_g u)}{\partial x} = \rho\mu_0(p_g - p_s), \quad \mu_0 > 0, \tag{40i}$$

$$\frac{\partial (\rho\eta_s)}{\partial t} + \mathrm{div}(\rho\eta_s\mathbf{v}) = \frac{(p_s - p_I)\dot{\alpha}_s}{Y_s\theta_s}, \tag{40j}$$

$$\frac{\partial (\rho\eta_g)}{\partial t} + \mathrm{div}(\rho\eta_g\mathbf{v}) = \frac{(p_g - p_I)\dot{\alpha}_g}{Y_g\theta_g}. \tag{40k}$$

System (40) admits the energy equation:

$$\begin{aligned}&\frac{\partial}{\partial t}\left(\rho\left(e + \frac{u^2 + v^2 + w^2}{2}\right)\right) \\ &\quad + \frac{\partial}{\partial x}\left(\rho u\left(e + \frac{u^2 + v^2 + w^2}{2}\right) - (\alpha_s\sigma_{s11} + \alpha_g\sigma_{g11})u - (\alpha_s\sigma_{s12} + \alpha_g\sigma_{g12})v - (\alpha_s\sigma_{s13} + \alpha_g\sigma_{g13})v\right) = 0,\end{aligned} \tag{41}$$

where

$$\rho e = \rho\left(Y_g e_g\left(\frac{Y_g\rho}{\alpha_g},\frac{\rho\eta_g}{\rho}\right)+Y_s\varepsilon_s^h\left(\frac{Y_s\rho}{1-\alpha_g},\frac{\rho\eta_s}{\rho}\right)\right)+\rho_{s0}|\langle G\rangle|^{1/2}\varepsilon_s^e\left(\frac{\langle G\rangle}{|\langle G\rangle|^{1/3}}\right), \tag{42}$$

Let us recall the following general result: if a system of conservation laws

$$\mathbf{V}_t+\mathbf{G}(\mathbf{V})_x=\mathbf{0}, \tag{43}$$

admits an additional conservation law

$$\varphi(\mathbf{V})_t+\psi(\mathbf{V})_x=0,$$

where $\varphi(\mathbf{V})$ is a convex function of $\mathbf{V}$, the system (43) is hyperbolic (see [17] for detail). In our case this function $\varphi$ is the total volume energy defined from (41):

$$E=\rho\left(e+\frac{u^2+v^2+w^2}{2}\right),$$

and $\mathbf{V}=(A^{(\beta)},\rho,\rho Y_g,\rho u,\rho v,\rho w,\rho\alpha_g,\rho\eta_s,\rho\eta_g)^T$. A difficulty to apply directly the result by Godunov et al. is that the convexity condition is difficult to check for a large number of variables. Let us remark that the equations for the volume and mass fractions, and the entropies evolve along contact characteristics. Hence, for hyperbolicity it is sufficient to check the convexity of the energy with respect to a lower number of variables $\widehat{\mathbf{V}}=(A^{(\beta)},\rho,\rho u,\rho v,\rho w)^T$. The total energy is in the form:

$$E=\mathscr{E}^k(\rho,\rho u,\rho v,\rho w)+\mathscr{E}^h(\rho,\alpha_g,Y_g,\eta_g,\eta_s)+\mathscr{E}_s^e(A^{(1)},A^{(2)},A^{(3)})$$

where the kinetic, hydrodynamic and elastic parts of the volume energy are defined as:

$$\mathscr{E}^k(\rho,\rho u,\rho v,\rho w)=\frac{(\rho u)^2+(\rho v)^2+(\rho w)^2}{2\rho},$$

$$\mathscr{E}^h(\rho,\alpha_g,Y_g,\eta_g,\eta_s)=\rho Y_g\varepsilon_g^h\left(\rho\frac{Y_g}{\alpha_g},\eta_g\right)+\rho Y_s\varepsilon_s^h\left(\rho\frac{(1-Y_g)}{(1-\alpha_g)},\eta_s\right),$$

$$\mathscr{E}_s^e(A^{(1)},A^{(2)},A^{(3)})=\rho_{s0}|\langle G\rangle|^{1/2}\varepsilon_s^e\left(\frac{\langle G\rangle}{|\langle G\rangle|^{1/3}}\right).$$

The energy $E$ is a convex function of $\widehat{\mathbf{V}}$, if

$$\frac{\mathscr{E}^k+\mathscr{E}^h}{\rho}=\frac{u^2+v^2+w^2}{2}+Y_g\varepsilon_g^h+Y_g\varepsilon_s^h,$$

is convex with respect to $(\tau=1/\rho,u,v,w)$, and

$$\mathscr{E}_s^e=\rho_{s0}|\langle G\rangle|^{1/2}\varepsilon_s^e\left(\frac{\langle G\rangle}{|\langle G\rangle|^{1/3}}\right),$$

is convex with respect to $A^{(\beta)}$. The function $(\mathscr{E}^k+\mathscr{E}^h)/\rho$ is convex with respect $(\tau=1/\rho,u,v,w)$ if the hydrodynamic energies of pure phases $\varepsilon_g^h$ and $\varepsilon_s^h$ are convex with respect to $\tau_g$ and $\tau_s$, respectively. This is the case, for example, of the stiffened gas equation of state. To prove the convexity of $\mathscr{E}_s^e$ in the case where $\varepsilon_s^e$ is given by (11), let us remark that the energy is in the form

$$\begin{aligned}\mathscr{E}_s^e&=\frac{\mu_s}{4}|\langle G\rangle|^{1/2}tr\left(\left(\frac{\langle G\rangle}{|\langle G\rangle|^{1/3}}-I\right)^2\right)=\frac{\mu_s}{4}A^{(1)}\left(\frac{\langle J_2\rangle}{(A^{(1)})^{4/3}}-\frac{2\langle J_1\rangle}{(A^{(1)})^{2/3}}+3\right)\\&=\frac{\mu_s}{4}A^{(1)}\left(\frac{((A^{(1)})^2+(A^{(2)})^2+(A^{(3)})^2)^2+2((A^{(2)})^2+(A^{(3)})^2)+2}{(A^{(1)})^{4/3}}-\frac{2((A^{(1)})^2+(A^{(2)})^2+(A^{(3)})^2+2)}{(A^{(1)})^{2/3}}+3\right)\\&=\frac{\mu_s}{4}\left(\frac{((A^{(1)})^2+Z^2)^2+2Z^2+2}{(A^{(1)})^{1/3}}-2(A^{(1)})^{1/3}((A^{(1)})^2+Z^2+2)+3\right),\end{aligned}$$

where

$$Z^2=(A^{(2)})^2+(A^{(3)})^2.$$

If the energy $\mathscr{E}_s^e$ is convex with respect to $A^{(1)}$ and $Z$, and $\partial\mathscr{E}_s^e/\partial Z>0$, it will be convex with respect to $A^{(1)},A^{(2)}$ and $A^{(3)}$. Obviously,

$$\frac{\partial\mathscr{E}_s^e}{\partial Z}=\frac{\mu_s}{\left(A^{(1)}\right)^{1/3}}\left(Z^3+Z\left(\left(A^{(1)}\right)^2-\left(A^{(1)}\right)^{2/3}+1\right)\right)>0$$

since for any positive $x$ we have $x^3-x+1>0$. Finally, to prove the convexity of $\mathscr{E}_s^e$ with respect to variables $(A^{(1)},Z)$ we have to prove that the corresponding $2\times 2$ Hessian matrix is positive definite in all domain of parameters $Z>0,A^{(1)}>0$:

$$\begin{pmatrix} \frac{\partial^2 \mathscr{E}_s^e}{\partial (A^{(1)})^2} & \frac{\partial^2 \mathscr{E}_s^e}{\partial A^{(1)} \partial Z} \\ \frac{\partial^2 \mathscr{E}_s^e}{\partial A^{(1)} \partial Z} & \frac{\partial^2 \mathscr{E}_s^e}{\partial Z^2} \end{pmatrix} > 0.$$

The proof can be done by direct calculations or using any tool for symbolic computations. The symmetrization method assures the hyperbolicity, however it does not give the characteristic eigenvalues in explicit form. They can be calculated in the limit of small deformations ($A^{(1)} \approx 1, A^{(2)} \approx 0, A^{(3)} \approx 0, \alpha_s \approx \alpha_{s0}$):

$$v_{1,2} = u, \quad v_{3,4,5,6} = u \pm \sqrt{Y_{s0} \frac{\mu_s}{\rho_{s0}}}, \quad v_{7,8} = u \pm \sqrt{Y_{s0}\left(c_{s0}^2 + \frac{4}{3}\frac{\mu_s}{\rho_{s0}}\right) + Y_g c_{g0}^2}, \quad Y_{s0} = \frac{\alpha_{s0}\rho_{s0}}{\rho_0}, \quad Y_{g0} = \frac{(1-\alpha_{s0})\rho_{g0}}{\rho_0}.$$

Here, the index "zero" corresponds to the equilibrium state. The sound velocities are the frozen sound velocities corresponding to the longitudinal waves:

$$c_l^2 = Y_{s0}(c_{s0}^2 + \frac{4}{3}\frac{\mu_s}{\rho_{s0}}) + Y_{g0} c_{g0}^2,$$

and transversal waves:

$$c_t^2 = Y_{s0}\frac{\mu_s}{\rho_{s0}}.$$

Let us remark that in the limit where the solid phase is completely absent or the shear modulus $\mu_s$ vanishes, the model degenerates: it is no more hyperbolic. Even if the eigenvalues are always real, the system of eigenvectors is not complete. In practice, we avoid this degeneracy since a negligible quantity of the second phase is always present in a "pure" phase.

## 4. Numerical approximation of the pressure non-equilibrium diffuse interface model

### 4.1. Diffuse interface model in one-space dimension

The geometric non-conservative Eq. (21) is

$$\frac{D\mathbf{E}^\beta}{Dt} + \left(\frac{\partial \mathbf{v}}{\partial \mathbf{x}}\right)^T \mathbf{E}^\beta = 0.$$

Consider the one-dimensional case where all the variables depend only on $(x,t)$ and the velocity field has only two non-trivial components: $\mathbf{v} = (u, v, 0)^T$. We suppose that $A^{(3)} = B^{(3)} = C^{(1)} = C^{(2)} = 0, C^{(3)} = 1$. We do not suppose $B^{(1)} = 0$ and $B^{(2)} = 1$ for symmetry reasons. The system of governing equations is:

$$\frac{\partial \alpha_s}{\partial t} + u\frac{\partial \alpha_s}{\partial x} = \mu_0(p_s - p_g), \tag{44a}$$

$$\frac{\partial \alpha_g \rho_g e_g}{\partial t} + \frac{\partial \alpha_g \rho_g e_g u}{\partial x} - \alpha_g \sigma_{11g}\frac{\partial u}{\partial x} = -p_I \mu_0(p_g - p_s), \tag{44b}$$

$$\frac{\partial \alpha_s \rho_s e_s}{\partial t} + \frac{\partial \alpha_s \rho_s e_s u}{\partial x} - \alpha_s \sigma_{11s}\frac{\partial u}{\partial x} - \alpha_s \sigma_{12s}\frac{\partial v}{\partial x} = -p_I \mu_0(p_s - p_g), \tag{44c}$$

$$\frac{\partial A^{(1)}}{\partial t} + \frac{\partial A^{(1)} u}{\partial x} + B^{(1)}\frac{\partial v}{\partial x} = 0, \tag{44d}$$

$$\frac{\partial A^{(2)}}{\partial t} + \frac{\partial A^{(2)} u}{\partial x} + B^{(2)}\frac{\partial v}{\partial x} = 0, \tag{44e}$$

$$\frac{\partial B^{(1)}}{\partial t} + u\frac{\partial B^{(1)}}{\partial x} = 0, \tag{44f}$$

$$\frac{\partial B^{(2)}}{\partial t} + u\frac{\partial B^{(2)}}{\partial x} = 0, \tag{44g}$$

$$\frac{\partial \alpha_s \rho_s}{\partial t} + \frac{\partial \alpha_s \rho_s u}{\partial x} = 0, \tag{44h}$$

$$\frac{\partial \alpha_g \rho_g}{\partial t} + \frac{\partial \alpha_g \rho_g u}{\partial x} = 0, \tag{44i}$$

$$\frac{\partial \rho u}{\partial t} + \frac{\partial \rho u^2 - (\alpha_g \sigma_{11g} + \alpha_s \sigma_{11s})}{\partial x} = 0, \tag{44j}$$

$$\frac{\partial \rho v}{\partial t} + \frac{\partial \rho u v - (\alpha_g \sigma_{12g} + \alpha_s \sigma_{12s})}{\partial x} = 0, \tag{44k}$$

$$\frac{\partial \left(\rho\left(Y_s e_s + Y_g e_g + \frac{1}{2}u^2 + \frac{1}{2}v^2\right)\right)}{\partial t} + \frac{\partial \left(u\left(\rho\left(Y_s e_s + Y_g e_g + \frac{1}{2}u^2\right) - (\alpha_g \sigma_{11g} + \alpha_s \sigma_{11s})\right) - (\alpha_g \sigma_{12g} + \alpha_s \sigma_{12s})v\right)}{\partial x} = 0. \tag{44l}$$

Thermodynamic closure is achieved by taking the following equations of state for the gas phase:

$$\alpha_g \rho_g \varepsilon_g^h = \frac{\alpha_g (p_g + \gamma_g p_{\infty g})}{(\gamma_g - 1)}, \tag{45}$$

and for the solid phase:

$$\alpha_s \rho_s \varepsilon_s^h = \frac{\alpha_s (p_s + \gamma_s p_{\infty s})}{(\gamma_s - 1)}, \quad \alpha_s \rho_s \varepsilon_s^e = \frac{\mu_s}{4|\langle G\rangle|^{1/6}} tr\Big((\langle G\rangle - |\langle G\rangle|^{1/3} I)^2\Big). \tag{46}$$

with $\langle G\rangle$ given by:

$$\langle G\rangle = \begin{pmatrix} (A^{(1)})^2 + (A^{(2)})^2 & A^{(1)}B^{(1)} + A^{(2)}B^{(2)} & 0 \\ A^{(1)}B^{(1)} + A^{(2)}B^{(2)} & (B^{(1)})^2 + (B^{(2)})^2 & 0 \\ 0 & 0 & 1 \end{pmatrix}.$$

The averaged solid stress tensor is:

$$\alpha_s \sigma_s = -\alpha_s p_s I - \frac{\mu_s}{|\langle G\rangle|^{1/6}} \left( \langle G\rangle^2 - \frac{\langle J_2\rangle}{3} I - |\langle G\rangle|^{1/3} \left( \langle G\rangle - \frac{\langle J_1\rangle}{3} I \right) \right), \quad \langle J_m\rangle = tr(\langle G\rangle^m), \quad m = 1, 2.$$

These relations are rewritten as a function of $A^{(\beta)}, B^{(\beta)}$ in Appendix C. The averaged stress tensor for the gas phase is trivial:

$$\alpha_g \sigma_g = -\alpha_g p_g I.$$

#### 4.1.1. Characteristic speeds

In absence of relaxation terms, this system can alternatively be written in primitive variables

$$\mathbf{W} = \left(\alpha_s, \rho_s, \rho_g, u, v, p_s, p_g, A^{(1)}, A^{(2)}, B^{(1)}, B^{(2)}\right)^T,$$

under the form:

$$\frac{\partial \mathbf{W}}{\partial t} + \mathbf{A}(\mathbf{W}) \frac{\partial \mathbf{W}}{\partial \mathbf{x}} = \mathbf{0}, \tag{47}$$

where

$$A = \begin{pmatrix} u & 0 & 0 & 0 & 0 & 0 & 0 & 0 & 0 & 0 & 0 \\ 0 & u & 0 & \rho_s & 0 & 0 & 0 & 0 & 0 & 0 & 0 \\ 0 & 0 & u & \rho_g & 0 & 0 & 0 & 0 & 0 & 0 & 0 \\ \frac{p_s - p_g}{\rho} & 0 & 0 & u & 0 & \frac{\alpha_s}{\rho} & \frac{\alpha_g}{\rho} & -\frac{1}{\rho}\frac{\partial(\alpha_s \sigma_{11s})}{\partial A^{(1)}} & -\frac{1}{\rho}\frac{\partial(\alpha_s \sigma_{11s})}{\partial A^{(2)}} & -\frac{1}{\rho}\frac{\partial(\alpha_s \sigma_{11s})}{\partial B^{(1)}} & -\frac{1}{\rho}\frac{\partial(\alpha_s \sigma_{11s})}{\partial B^{(2)}} \\ 0 & 0 & 0 & 0 & u & 0 & 0 & -\frac{1}{\rho}\frac{\partial(\alpha_s \sigma_{12s})}{\partial A^{(1)}} & -\frac{1}{\rho}\frac{\partial(\alpha_s \sigma_{12s})}{\partial A^{(2)}} & -\frac{1}{\rho}\frac{\partial(\alpha_s \sigma_{12s})}{\partial B^{(1)}} & -\frac{1}{\rho}\frac{\partial(\alpha_s \sigma_{12s})}{\partial B^{(2)}} \\ 0 & 0 & 0 & \rho_s c_s^2 & 0 & u & 0 & 0 & 0 & 0 & 0 \\ 0 & 0 & 0 & \rho_g c_g^2 & 0 & 0 & u & 0 & 0 & 0 & 0 \\ 0 & 0 & 0 & A^{(1)} & B^{(1)} & 0 & 0 & u & 0 & 0 & 0 \\ 0 & 0 & 0 & A^{(2)} & B^{(2)} & 0 & 0 & 0 & u & 0 & 0 \\ 0 & 0 & 0 & 0 & 0 & 0 & 0 & 0 & 0 & u & 0 \\ 0 & 0 & 0 & 0 & 0 & 0 & 0 & 0 & 0 & 0 & u \end{pmatrix}.$$

Here, the sound velocities $c_s$ and $c_g$ are determined only by the hydrodynamic part of energy:

$$c_s^2 = \gamma_s \frac{p_s + p_{\infty s}}{\rho_s}, \quad c_g^2 = \gamma_g \frac{p_g + p_{\infty g}}{\rho_g}.$$

The characteristic wave speeds are solutions of the following polynomial:

$$(u - v)^4 + (u - v)^2 \left( \frac{\alpha_s \left( A^{(1)} \frac{\partial \sigma_{11s}}{\partial A^{(1)}} + A^{(2)} \frac{\partial \sigma_{11s}}{\partial A^{(2)}} + B^{(1)} \frac{\partial \sigma_{12s}}{\partial A^{(1)}} + B^{(2)} \frac{\partial \sigma_{12s}}{\partial A^{(2)}} \right) - (\alpha_s \rho_s c_s^2 + \alpha_g \rho_g c_g^2)}{\rho} \right)$$
$$+ \alpha_s \left( \frac{(A^{(1)}B^{(2)} - B^{(1)}A^{(2)}) \left( \frac{\partial \sigma_{11s}}{\partial A^{(1)}} \frac{\partial \sigma_{12s}}{\partial A^{(2)}} - \frac{\partial \sigma_{11s}}{\partial A^{(2)}} \frac{\partial \sigma_{12s}}{\partial A^{(1)}} \right) \alpha_s}{\rho^2} - \frac{\left( B^{(1)} \frac{\partial \sigma_{12s}}{\partial A^{(1)}} + B^{(2)} \frac{\partial \sigma_{12s}}{\partial A^{(2)}} \right) (\alpha_g \rho_g c_g^2 + \alpha_s \rho_s c_s^2)}{\rho^2} \right) = 0.$$

In the limit of small deformations ($A^{(1)} \approx 1, A^{(2)} \approx 0, B^{(1)} \approx 0, B^{(2)} \approx 1$) we obtain previously the eigenvalues

$$u, \quad u \pm \sqrt{Y_s \frac{\mu_s}{\rho_s}}, \quad u \pm \sqrt{Y_s\left(c_s^2 + \frac{4}{3}\frac{\mu_s}{\rho_s}\right) + Y_g c_g^2}.$$

Our numerical strategy relies the Godunov type schemes with approximate Riemann solvers. Among them, the HLLC solver Toro et al. [34] and Toro [35], is of specific interest because it preserves volume fraction and density positivity, and is able to deal with strong discontinuities. With this solver, each wave is considered as a discontinuity and, consequently, jump relations are needed. The system being non-conservative, shock relations are non-conventional.

*4.1.2. Shock relations*

In Saurel et al. [30] approximate shock relations have been derived for a non-equilibrium diffuse interface model of compressible fluids. We will adapt them to the diffuse solid–fluid interface model. It is necessary that the Rankine–Hugoniot relations verify the following properties:

- Single phase limit is recovered for which jump relations are unambiguously known.
- Conservation of the mass, momentum and energy of the mixture are satisfied.
- Second law of thermodynamics for the mixture is satisfied.

Below, we propose a set of Rankine–Hugoniot relations which fulfils these requirements and, as will be shown later, the relations are accurate enough to reach convergence for solid–fluid interface problems.

*4.1.2.1. Jump relations for conserved variables.* Jump relations for the mass equations are:

$$\alpha_s \rho_s (u - D) = \alpha_s^0 \rho_s^0 (u^0 - D) = m_s, \tag{48}$$

$$\alpha_g \rho_g (u - D) = \alpha_g^0 \rho_g^0 (u^0 - D) = m_g, \tag{49}$$

In particular, the mass fraction is continuous through the jump:

$$Y_k = Y_{k0}, \quad k = s, g.$$

The variables with superscript "0" denote the unshocked state. The speed of the discontinuity is denoted by $D$. Let us denote by

$$\sigma_{11} = \alpha_s \sigma_{11s} + \alpha_g \sigma_{11g},$$
$$\sigma_{12} = \alpha_s \sigma_{12s} + \alpha_g \sigma_{12g}$$

the mixture normal and tangential stresses, and

$$m = m_s + m_g,$$

the mixture mass flux. With these notations, the momentum jump relations read:

$$\sigma_{11} - \sigma_{11}^0 - m^2(\tau - \tau^0) = 0, \tag{50}$$

$$\sigma_{12} - \sigma_{12}^0 - m(v - v^0) = 0. \tag{51}$$

The mixture energy jump condition reads:

$$e - e^0 = \frac{1}{2}(\tau - \tau^0)(\sigma_{11} + \sigma_{11}^0) + \frac{1}{2}\left(\tau^0 (A^{(2)})^0 - \tau A^{(2)}\right)(\sigma_{12} + \sigma_{12}^0), \tag{52}$$

with $e = Y_s e_s + Y_g e_g$ and $\tau = Y_g \tau_g + Y_s \tau_s, \tau_k = 1/\rho_k$.

*4.1.2.2. Jump relations for geometrical variables.* In absence of relaxation effects, the geometric equations read:

$$\frac{\partial A^{(1)}}{\partial t} + \frac{\partial A^{(1)} u}{\partial x} + B^{(1)} \frac{\partial v}{\partial x} = 0, \tag{53}$$

$$\frac{\partial A^{(2)}}{\partial t} + \frac{\partial A^{(2)} u}{\partial x} + B^{(2)} \frac{\partial v}{\partial x} = 0, \tag{54}$$

$$\frac{\partial B^{(1)}}{\partial t} + u \frac{\partial B^{(1)}}{\partial x} = 0, \tag{55}$$

$$\frac{\partial B^{(2)}}{\partial t} + u \frac{\partial B^{(2)}}{\partial x} = 0. \tag{56}$$

It follows from (55) and (56) that we have the following invariants across left- and right-facing waves:

$$B^{(1)} = (B^{(1)})^0,$$
$$B^{(2)} = (B^{(2)})^0.$$

Thus, there is no difficulty to determine jump relations for (53) and (54):

$$A^{(1)}(u-D)+B^{(1)}v=(A^{(1)}(u-D)+B^{(1)}v)^0,$$
$$A^{(2)}(u-D)+B^{(2)}v=(A^{(2)}(u-D)+B^{(2)}v)^0.$$

*4.1.2.3. Jump relations for non-conservative variables.* The volume fraction is continuous through the jump:

$$\alpha_k=\alpha_k^0,\quad k=g,s$$

The internal energy equations being in non-conservative form, they are not adapted to the determination of jump relations. The following jump relations are then proposed:

$$e_k-e_k^0=\frac{1}{2}(\tau_k-\tau_k^0)(\sigma_{11k}+\sigma_{11k}^0)+\frac{1}{2}\left(\tau_k^0(A^{(2)})^0-\tau_k(A^{(2)})\right)(\sigma_{12k}+\sigma_{12k}^0),\quad k=g,s. \tag{57}$$

We now examine the conditions that have to be fulfilled.

– Single phase limit.

When the solid volume fraction tends to zero, the preceding jump relation has to tend to the energy jump relation for the Euler equations. This condition is fulfilled because $\sigma_{12g}$ is zero is the gas and $\sigma_{11g}=-p_g$. When the gas volume fraction tends to zero, the mixture jump condition (52) is equivalent to the solid phase jump (57).

– Energy conservation

Multiplying each Eq. (57) by $Y_k=\alpha_k\rho_k/\rho$ and summing them we obtain:

$$\begin{aligned}&Y_s(e_s-e_s^0)-\frac{\sigma_{11s}+\sigma_{11s}^0}{2}(Y_s\tau_s-Y_s\tau_s^0)+Y_g(e_g-e_g^0)-\frac{\sigma_{11g}+\sigma_{11g}^0}{2}\left(Y_g\tau_g-Y_g\tau_g^0\right)\\&-\left((A^{(2)})^0Y_s\tau_s^0-A^{(2)}Y_s\tau_s\right)\frac{(\sigma_{12s}+\sigma_{12s}^0)}{2}-\left((A^{(2)})^0Y_g\tau_g^0-A^{(2)}Y_g\tau_g\right)\frac{(\sigma_{12g}+\sigma_{12g}^0)}{2}\\&=0.\end{aligned}$$

Or

$$e-e^0-\frac{\alpha_s\sigma_{11s}+\alpha_g\sigma_{11g}+\alpha_s\sigma_{11s}^0+\alpha_g\sigma_{11g}^0}{2}(\tau-\tau^0)-\left((A^{(2)})^0\tau^0-A^{(2)}\tau\right)\left(\frac{\alpha_s\sigma_{12s}+\alpha_g\sigma_{12g}+\alpha_s\sigma_{12s}^0+\alpha_g\sigma_{12g}^0}{2}\right)=0.$$

This is equivalent to (52). With the help of these relations, approximate Riemann solvers can be built as developed hereafter.

*4.1.3. Interface relations*

Consider system (44l) in absence of relaxation terms. Eqs. (53) and (54) show that if the terms $B^{(1)}$ and $B^{(2)}$ are discontinuous across contact discontinuities, then necessarily the tangential velocity should be continuous, $[v]=0$. If not the non-conservative product is not well defined. Thus, the resulting set of interface relations is:

$$[u]=0, \tag{58a}$$
$$[v]=0\quad\text{if}\quad\alpha_s\neq0, \tag{58b}$$
$$[v]\neq0\quad\text{if}\quad\alpha_s=0, \tag{58c}$$
$$[\sigma_{11}]=[\alpha_g\sigma_{11g}+\alpha_s\sigma_{11s}]=0, \tag{58d}$$
$$[\sigma_{12}]=[\alpha_s\sigma_{12s}+\alpha_g\sigma_{12g}]=0. \tag{58e}$$

A difficulty appears with system (58e). When an interface appears between two solid states, the jump condition $[v]=0$ holds. This is not the case in the situation where an interface separates two fluid states and where $[v]\neq0$. When an interface separates solid and fluid states ($\alpha_s\approx0$), the sliding between components is possible. However, it will necessitate a specific numerical treatment. This issue will be addressed later.

*4.2. HLLC type Riemann solver*

Consider a cell boundary separating a left state ($L$) and a right state ($R$). The left- and right-facing wave speeds are obtained following Davis [9] estimates:

$$S_R=\max(u_L+c_L,u_R+c_R),$$
$$S_L=\min(u_L-c_L,u_R-c_R).$$

where $c_{L,R}$ are the longitudinal sound speed of the mixture: $c^2 = Y_s c_{ls}^2 + Y_g c_g^2$ with $c_{ls}$ the longitudinal wave speed in the pure solid. We consider only three waves and not five waves because, as it was shown in [14], the Godunov method with HLLC solver will be able to capture all these waves. The speed of the intermediate wave (or contact discontinuity) is estimated under HLL approximation:

$$S_M = \frac{(\rho u^2 - \sigma_{11})_L - (\rho u^2 - \sigma_{11})_R - S_L(\rho u)_L + S_R(\rho u)_R}{(\rho u)_L - (\rho u)_R - S_L\rho_L + S_R\rho_R} = u^*,$$

with the mixture normal stress $\sigma_{11} = \alpha_s\sigma_{11(s)} + \alpha_g\sigma_{11(g)}$ and mixture density $\rho = \alpha_s\rho_s + \alpha_g\rho_g$ defined previously.

From these wave speeds conservative state variables in the star region (see Fig. 3) are determined:

$$(\alpha_k\rho_k)^*_{L,R} = (\alpha_k\rho_k)_{L,R}\frac{S_{L,R} - u_{L,R}}{S_{L,R} - u^*},$$

$$\sigma^*_{11} = \frac{(u_R - S_R)\rho_R\sigma_{11L} - (u_L - S_L)\rho_L\sigma_{11R} + (u_L - S_L)\rho_L(u_R - S_R)\rho_R(u_R - u_L)}{(u_R - S_R)\rho_R - (u_L - S_L)\rho_L},$$

$$\sigma^*_{12} = \frac{(u_R - S_R)\rho_R\sigma_{12L} - (u_L - S_L)\rho_L\sigma_{12R} + (u_L - S_L)\rho_L(u_R - S_R)\rho_R(v_R - v_L)}{(u_R - S_R)\rho_R - (u_L - S_L)\rho_L},$$

$$v^*_{L,R} = v_{L,R} + \frac{(\sigma_{12})^* - (\sigma_{12})_{L,R}}{(u_{L,R} - S_{L,R})\rho_{L,R}} = v_{L,R} + \frac{(\alpha_s\sigma_{12s})^* - (\alpha_s\sigma_{12s})_{L,R}}{(u_{L,R} - S_{L,R})\rho_{L,R}};$$

The components $v^*_L$ and $v^*_R$ are equal for the case of a solid–solid contact discontinuity. But we prefer to make a distinction between them, as they will be different in the case of a solid–fluid contact. The right and the left mixture total energies are obtained as:

$$E^*_{L,R} = \frac{\rho_{L,R}E_{L,R}(u_{L,R} - S_{L,R}) - \sigma_{11L,R}u_{L,R} - \sigma_{12L,R}v_{L,R} + \sigma^*_{11}u^* + \sigma^*_{12}v^*_{L,R}}{\rho^*_{L,R}(u^* - S_{L,R})},$$

with

$$E = Y_s e_s + Y_g e_g + \frac{1}{2}u^2 + \frac{1}{2}v^2.$$

Then, the **geometrical variables** are determined as:

$$(A^{(1)})^*_{L,R} = \frac{A^{(1)}_{L,R}(u_{L,R} - S_{L,R}) + B^{(1)}_{L,R}(v_{L,R} - v^*_{L,R})}{u^* - S_{L,R}}, \quad (A^{(2)})^*_{L,R} = \frac{A^{(2)}_{L,R}(u_{L,R} - S_{L,R}) + B^{(2)}_{L,R}(v_{L,R} - v^*_{L,R})}{u^* - S_{L,R}},$$

$$(B^{(1)})^*_{L,R} = B^{(1)}_{L,R}, \quad (B^{(2)})^*_{L,R} = B^{(2)}_{L,R}$$

The **non-conservative variables** are finally determined:

$$\alpha^*_{kL,R} = \alpha_{kL,R}, \quad \alpha^*_{kL,R} = \alpha_{kL,R},$$

$$\rho^*_{kL,R} = \rho^0_{kL,R}\frac{u_{L,R} - S_{L,R}}{S_M - S_{L,R}}, \quad k = s, g.$$

The jumps of the internal energies are determined with the help of Hugoniots (57). Indeed, for example, with equations of state (45) and (46), the phase pressures $p^*_{kL,R}$ are calculated as functions of the phases densities $\rho^*_{kL,R}$ and (for $k = s$) geometrical variables $(A^{(\beta)})^*_{L,R}, (B^{(\beta)})^*_{L,R}$ along their respective Hugoniot curves defined by (57). Then the internal energies are determined as:

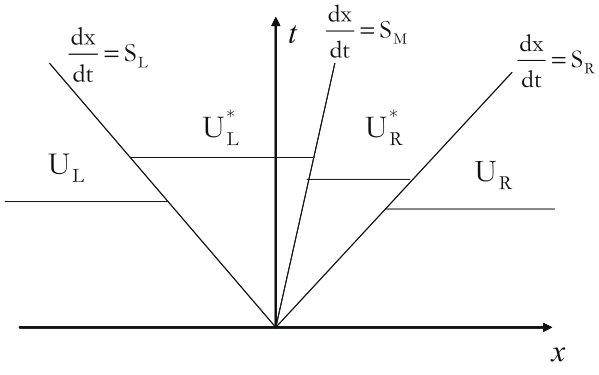


**Fig. 3.** HLLC approximate solver. Solution in the "star" region consists of two constant states separated from each other by a middle wave of speed $S_M$.

$$e^*_{gL,R} = e_g(p^*_{gL,R}, \rho^*_{gL,R}),$$
$$e^*_{sL,R} = e_s(p^*_{sL,R}, \rho^*_{sL,R}, (A^{(1)})^*_{L,R}, (A^{(2)})^*_{L,R}, (B^{(1)})^*_{L,R}, (B^{(2)})^*_{L,R})$$

With the help of this approximate solver, it is possible to derive a Godunov type scheme.

### 4.3. Godunov type method

The method used to solve interface problems with the diffuse interface formulation (44l) consists in a sequence of steps. The system contains conservative and non-conservative equations, as well as relaxation terms. The algorithm follows the one presented in Saurel et al. [30] in a simplified situation involving two fluids.

#### 4.3.1. Hyperbolic step

The conservative part of system (44l), in absence of relaxation terms is updated with the conventional Godunov scheme:

$$\mathbf{U}_i^{n+1} = \mathbf{U}_i^n - \frac{\Delta t}{\Delta x}(\mathbf{F}_1^*(\mathbf{U}_i^n, \mathbf{U}_{i+1}^n) - \mathbf{F}_1^*(\mathbf{U}_{i-1}^n, \mathbf{U}_i^n)), \tag{59}$$

with

$$\mathbf{U} = ((\alpha\rho)_s, (\alpha\rho)_g, \rho u, \rho v, \rho E)^T,$$

and

$$\mathbf{F}_1 = ((\alpha\rho)_s u, (\alpha\rho)_g u, \rho u^2 - \sigma_{11}, \rho u v - \sigma_{12}, (\rho E - \sigma_{11})u - \sigma_{12} v)^T.$$

The non-conservative part of system (44l), in absence of relaxation terms reads:

$$\frac{\partial \mathbf{G}}{\partial t} + \frac{\partial \mathbf{F}_2}{\partial x} + \mathbf{H}_2 \frac{\partial u}{\partial x} + \mathbf{K}_2 \frac{\partial v}{\partial x} = 0, \tag{60}$$

with

$$\mathbf{G} = (\alpha_s, A^{(1)}, B^{(1)}, A^{(2)}, B^{(2)}, \alpha_s\rho_s e_s, \alpha_g\rho_g e_g)^T,$$
$$\mathbf{F}_2 = (\alpha_s u, A^{(1)}u, B^{(1)}u, A^{(2)}u, B^{(2)}u, \alpha_s\rho_s e_s u, \alpha_g\rho_g e_g u)^T,$$
$$\mathbf{H}_2 = (-\alpha_s, 0, -B^{(1)}, 0, -B^{(2)}, -\alpha_s\sigma_{11s}, -\alpha_g\sigma_{11g})^T,$$
$$\mathbf{K}_2 = (0, B^{(1)}, 0, B^{(2)}, 0, -\alpha_s\sigma_{12s}, -\alpha_g\sigma_{12g})^T.$$

The non-conservative equations are solved by the following scheme, already used in Saurel et al. [30] to estimate volume fractions and internal energy equations:

$$\mathbf{G}_i^{n+1} = \mathbf{G}_i^n + \frac{\Delta t}{\Delta x}\left(\left(\mathbf{F}^*_{2i-1/2} - \mathbf{F}^*_{2i+1/2}\right) + \mathbf{H}^n_{2i}\left(u^*_{i-1/2} - u^*_{i+1/2}\right) + \mathbf{K}^n_{2i}\left(v^*_{i-1/2R} - v^*_{i+1/2L}\right)\right),$$

where $\mathbf{F}^*_{2i-1/2}$ and $\mathbf{F}^*_{2i+1/2}$ are the fluxes calculated on each cell boundary with the help of the HLLC solver. The normal velocity components $u^*_{i-1/2}$ and $u^*_{i+1/2}$ are also solution of the Riemann problem at the same cell boundaries, $v^*_{i-1/2R}$ and $v^*_{i+1/2L}$ are the corresponding tangential velocity components at the right and left sides of the contact discontinuity.

Eqs. (59) and (60) can be rewritten under the following form:

$$\frac{\partial \mathbf{V}}{\partial t} + \frac{\partial \mathbf{F}}{\partial x} + \mathbf{H}\frac{\partial u}{\partial x} + \mathbf{K}\frac{\partial v}{\partial x} = 0,$$

with $\mathbf{V}^T = (\mathbf{U}^T, \mathbf{G}^T)$ and $\mathbf{F}^T = (\mathbf{F}_1^T, \mathbf{F}_2^T), \mathbf{H}^T = (0,0,0,0,0,0,\mathbf{H}_2^T), \mathbf{K}^T = (0,0,0,0,0,0,\mathbf{K}_2^T)$. The following scheme is used for time evolution for all the equations:

$$\mathbf{V}_i^{n+1} = \mathbf{V}_i^n + \frac{\Delta t}{\Delta x}\left(\left(\mathbf{F}^*_{i-1/2} - \mathbf{F}^*_{i+1/2}\right) + \mathbf{H}^n_i\left(u^*_{i-1/2} - u^*_{i+1/2}\right) + \mathbf{K}^n_i\left(v^*_{i-1/2R} - v^*_{i+1/2L}\right)\right).$$

Regarding the non-conservative internal energy equations it is worth to mention that the adopted jump relations used in the Riemann solver will induce entropy jump in each phase in the presence of shocks. However, there is no hope that this jump be exact as the two-phase shock is smeared over several computational cells. Moreover, the evolution scheme (60) uses cell averages of non-conservative variables and simplified approximations for non-conservative products with $\mathbf{H}_i^n$ and $\mathbf{K}_i^n$ as local constants.

In order to correct this predicted solution, two extra steps are used. The first one corresponds to a pressure relaxation step, in order that mechanical equilibrium be reached everywhere and in particular at the interface. The second correction step corresponds to a reset of the internal energies with the help of the total energy conservation equation. These two correction steps are detailed hereafter.

*4.3.2. Relaxation step*

At the end of the hyperbolic step the two materials have different pressures. In order that mechanical equilibrium be restored in mixture cells, the relaxation step has to be done:

$$\frac{\partial \alpha_s}{\partial t} = \mu_0(p_s - p_g), \tag{61a}$$

$$\frac{\partial \alpha_g \rho_g e_g}{\partial t} = -p_I \mu_0(p_g - p_s), \tag{61b}$$

$$\frac{\partial \alpha_s \rho_s e_s}{\partial t} = p_I \mu_0(p_g - p_s), \tag{61c}$$

$$\frac{\partial A^{(\beta)}}{\partial t} = 0, \quad \frac{\partial B^{(\beta)}}{\partial t} = 0, \quad \beta = 1,2, \tag{61d}$$

$$\frac{\partial \alpha_k \rho_k}{\partial t} = 0, \quad k = s,g, \tag{61e}$$

$$\frac{\partial \rho u}{\partial t} = 0, \quad \frac{\partial \rho v}{\partial t} = 0, \quad \frac{\partial \rho E}{\partial t} = 0. \tag{61f}$$

Below, we will propose a simplified approach in the limit of stiff relaxation ($\mu_0 \to +\infty$). The phase energy equation can be rewritten in the following form:

$$\frac{\partial e_k}{\partial t} + p_I \frac{\partial \tau_k}{\partial t} = 0, \quad \tau_k = \frac{1}{\rho_k}.$$

Integrating this equation over the time interval, we can rewrite it in the algebraic form:

$$e_k^f - e_k^i - \hat{p}_{Ik}(\tau_k^f - \tau_k^i) = 0 \tag{62}$$

where indices "$f$" and "$i$" mean "final" (equilibrium) and "initial" (nonequilibrium) state. The non-equilibrium state is obtained after the first hyperbolic step. A new average interface pressure $\hat{p}_{Ik}$ appears here. Eq. (62) should imply the conservation of the mixture energy. A consequence of that is

$$\hat{p}_{Is} = \hat{p}_{Ig} = \hat{p}_I.$$

In general, $\hat{p}_I$ is different from $p_I$. However, as shown in Petitpas et al. [26], if the relaxation parameter $\mu_0$ is large, numerical results are insensitive to a particular choice of $\hat{p}_I$. It is convenient to use $\hat{p}_I = p^f$. Thus, using the algebraic energy equation and invariance properties of the material EOS, the phase specific volumes become functions only of pressure (see Appendix A):

$$\tau_k(p^f) = \tau_k^i \frac{p_k^i + \gamma_k p_{\infty,k} + p^f(\gamma_k - 1)}{p^f + \gamma_k p_{\infty,k} + p^f(\gamma_k - 1)}.$$

The closure of the model is achieved using the saturation constraint that reads:

$$\sum_k \alpha_k = 1,$$

or

$$\sum_k (\alpha\rho)_k \tau_k = 1. \tag{63}$$

In the limit $\mu_0 \to \infty$ system (61f) is reduced to an algebraic Eq. (63) to solve with $p^f$ as a single unknown. Once the relaxed pressure is determined, the phase volume fractions are deduced as well as the geometrical variables $(A^{(1)}, A^{(2)}, B^{(1)}, B^{(2)})$.

*4.3.3. Reinitialization step*

As the volume fractions have been estimated previously by the relaxation method, the mixture pressure can be determined from the mixture EOS based on the mixture energy which is known from the solution of the total energy equation. Because the mixture total energy obeys a conservation law, its evolution is accurate in the entire flow field and, in particular, at shocks. From the mixture total energy, we can extract the hydrodynamic part of the mixture internal energy:

$$\varepsilon^h = Y_s \varepsilon_s^h(p_s, \rho_s) + Y_g \varepsilon_g^h(p_g, \rho_g) = E - \frac{1}{2}u^2 - \frac{1}{2}v^2 - Y_s \varepsilon_s^e(A^{(1)}, A^{(2)}, B^{(1)}, B^{(2)}).$$

Again, considering fluids governed by the stiffened gas EOS and using the pressure equilibrium condition $p_s = p_g = p$, the mixture EOS now relates the mixture hydrodynamic internal energy, the mixture density and the volume fractions:

$$p(\rho, \varepsilon^h, \alpha_s, \alpha_g) = \frac{\rho\varepsilon^h - \left(\frac{\alpha_s\gamma_s p_{\infty s}}{\gamma_s - 1} + \frac{\alpha_g\gamma_g p_{\infty g}}{\gamma_g - 1}\right)}{\frac{\alpha_s}{\gamma_s - 1} + \frac{\alpha_g}{\gamma_g - 1}}. \tag{64}$$

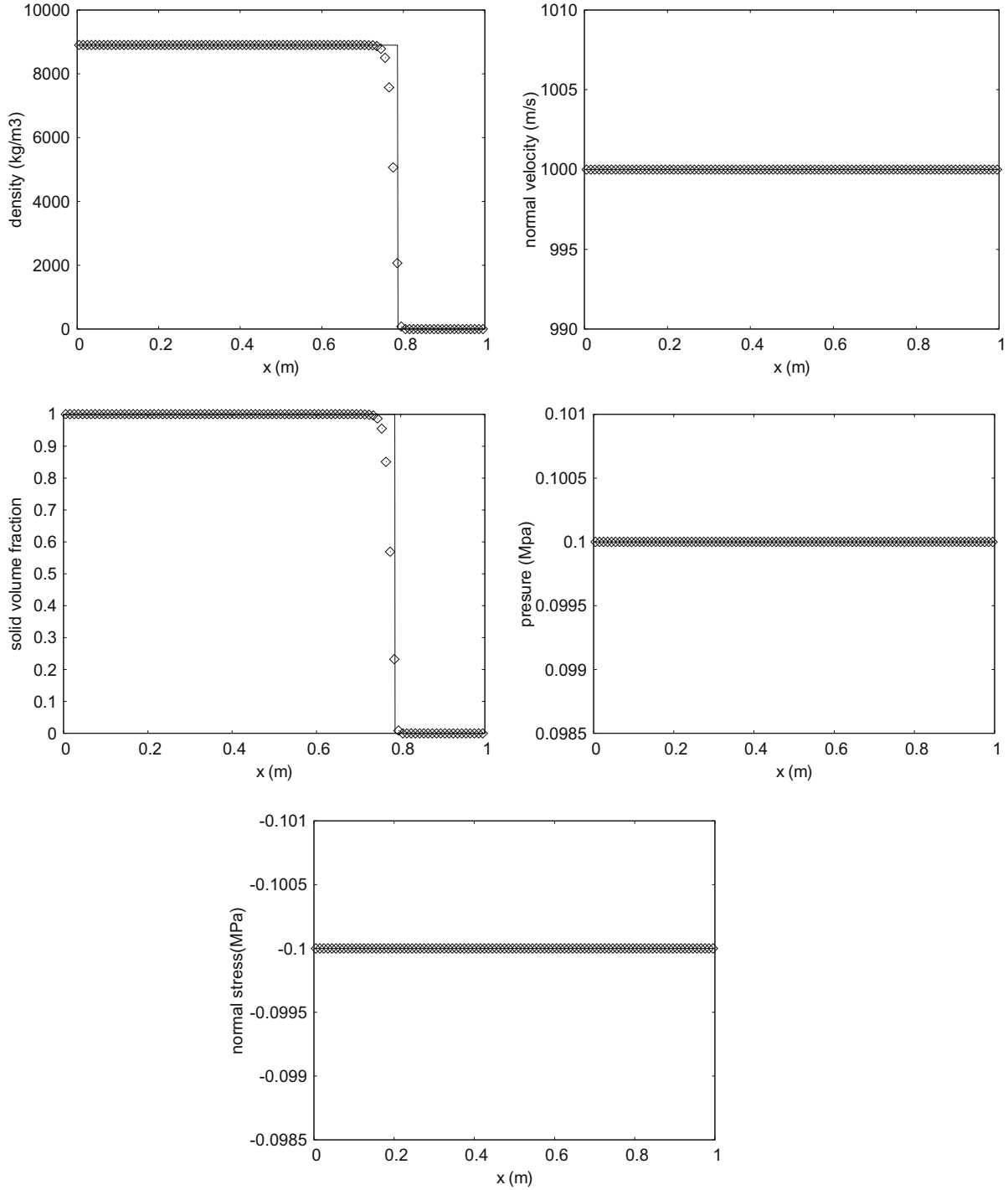


**Fig. 4.** Advection of a copper–air interface at uniform velocity ($u$ = 1000 m/s) under atmospheric conditions. The second-order variant of the method is used with Superbee limiter. The mesh involves 100 computational cells. The scheme preserves mechanical equilibrium as velocity and normal constraint fields are oscillation free.

Once the mixture pressure is determined the internal energies of the phases are reinitialized with the help of their respective EOS:

$$\varepsilon_k^h = \varepsilon_k^h\left(p, \frac{(\alpha_k\rho)_k}{\alpha_k}\right), \quad k = s,g \quad \varepsilon_s^e = \varepsilon_s^e\left(A^{(1)}, A^{(2)}, B^{(1)}, B^{(2)}\right).$$

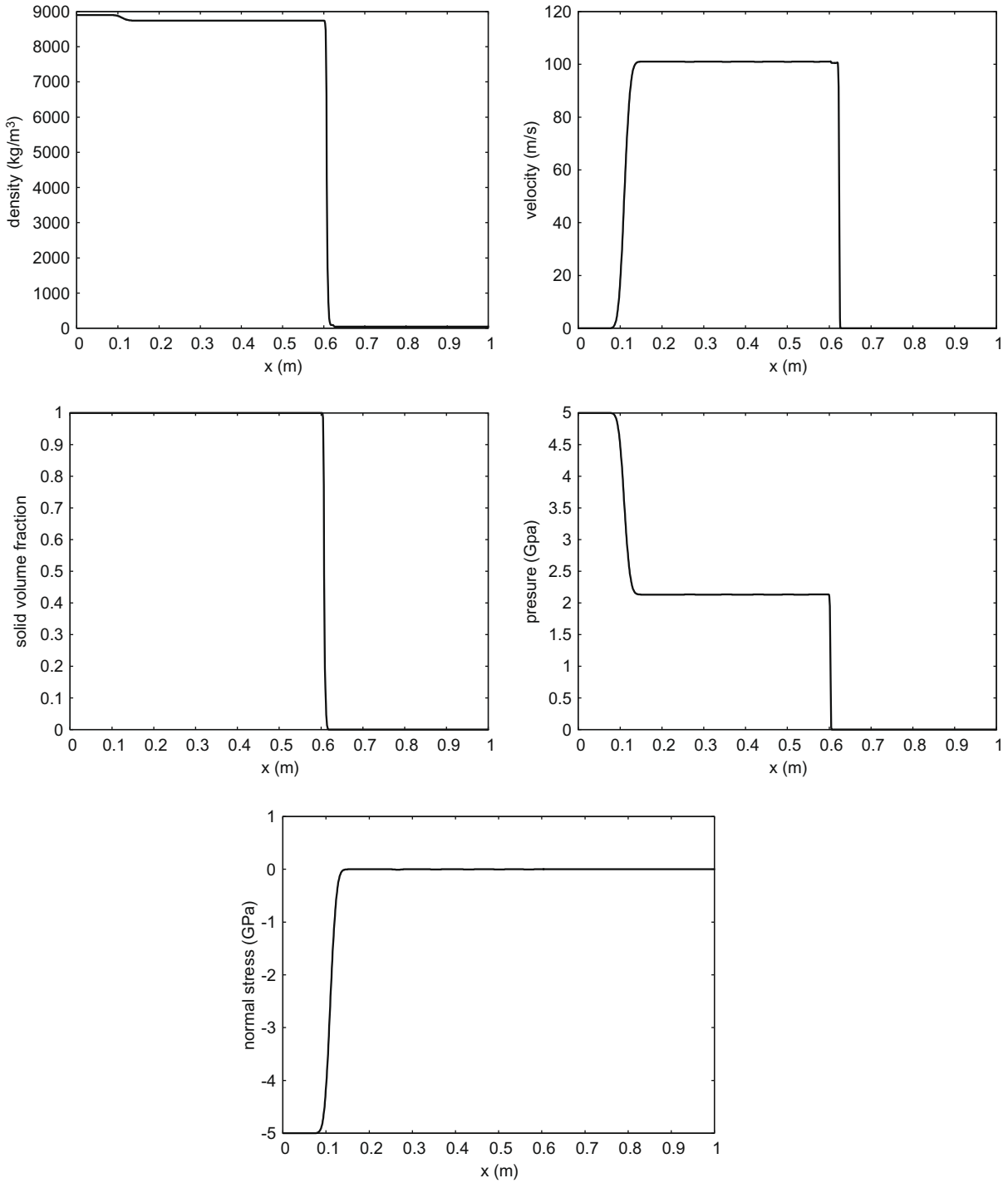


**Fig. 6.** Solid–gas shock tube with high pressure ($5.10^4$) and high density (178) ratios. The numerical solution is obtained with the second-order version of the method employing Minmod limiter. Computed results are shown with lines and involve 1000 computational cells. They illustrate robustness of the method.

*4.3.4. Summary*

The numerical method can be summarized as follows:

- At each cell boundary solve the Riemann problem for system (44l) without relaxation terms. The HLLC solver is recommended due to its simplicity, robustness and accuracy.
- Evolve all flow variables with the Godunov type method, higher order extension is developed in Appendix B.

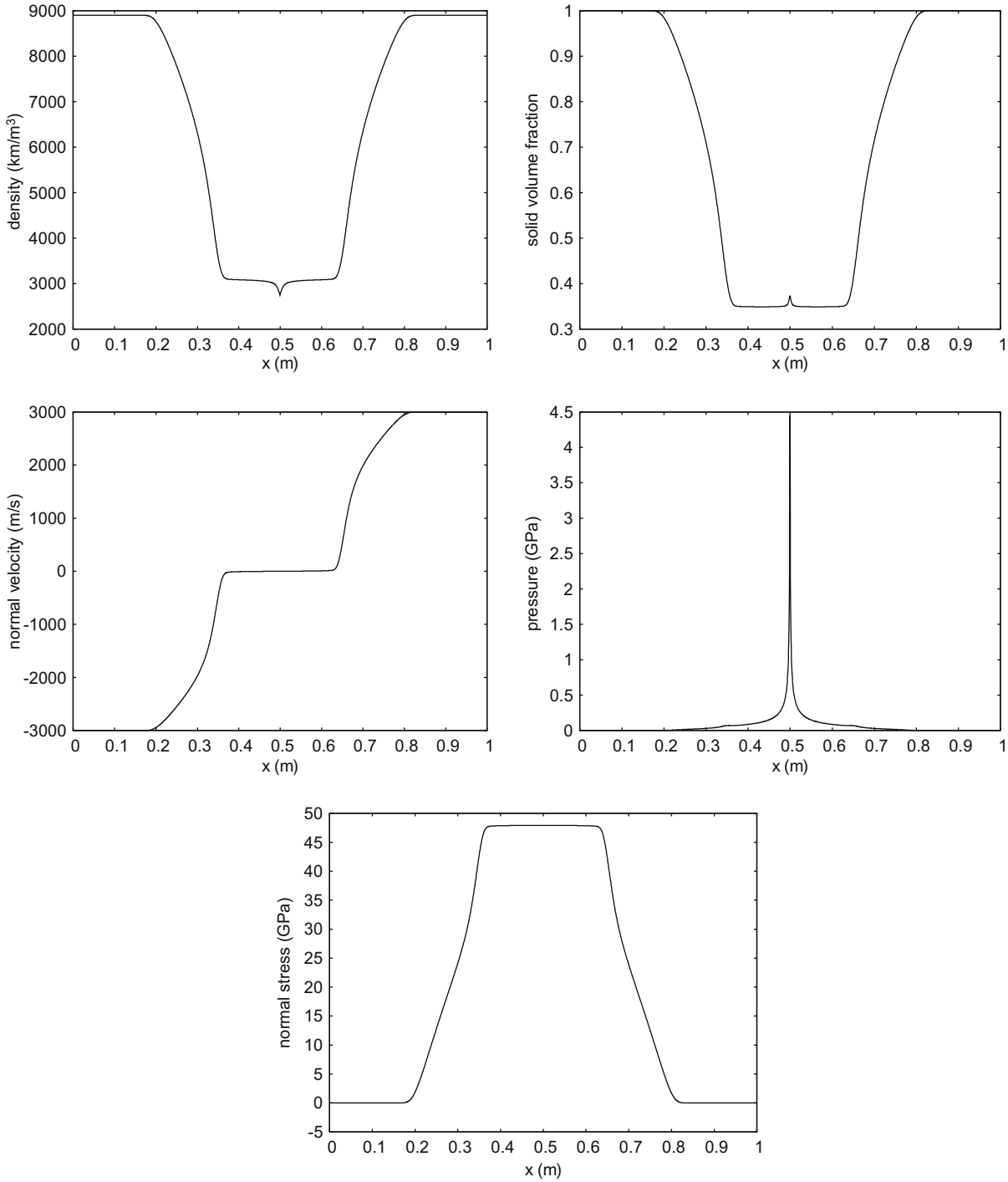


**Fig. 7.** Double expansion wave in copper. The initial velocity is $u = -3000$ m/s on the left part of the domain and is opposite on the right. A 2000 cells mesh is used with a second-order version of the method with Minmod limiter. A cavitation pocket appears dynamically and the pressure remains positive.

– Determine the relaxed pressure and especially the volume fractions by solving Eq. (63). The Newton method is appropriate for this task.
– Compute the mixture pressure using the Eq. (64).
– Reset the internal energies with the computed pressure with the help of their respective EOS.
– Start again for the next time step.

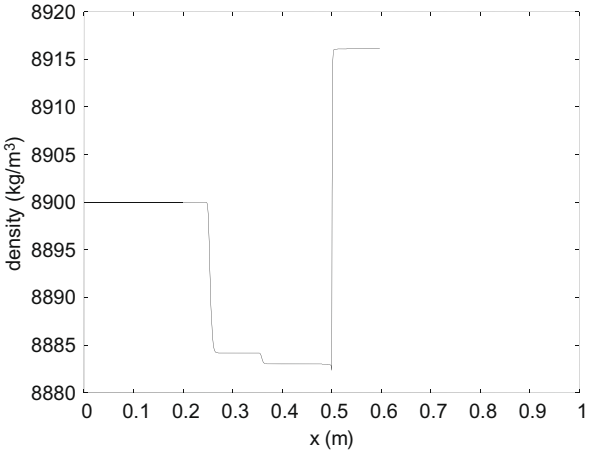

This method works very well as illustrated in the next section. However, when dealing with sliding effects at interfaces, some corrections have to be done as it will be shown further.

## 5. One-dimensional tests and validations

In all following test cases, the modeled solid has copper parameters with shear modulus $\mu_s = 9.2 \times 10^{10}$ Pa and initial density $\rho_{s0} = 8900$ kg/m$^3$. The thermodynamic part of the solid is governed by the stiffened gas equation with parameters $p_{\infty s} = 342.0 \times 10^8$ Pa and $\gamma_s = 4.22$. The fluid (water) is governed by the stiffened gas EOS with parameters $p_{\infty f} = 6.0 \times 10^8$ Pa and $\gamma_f = 4.4$, and the air when present is governed by the ideal gas EOS with parameter $\gamma_g = 1.4$.

### 5.1. Advection of a solid–gas interface

We consider a shock tube with solid copper at the density $\rho = 8900$ kg/m$^3$on the left and air with the density $\rho = 1$ kg/m$^3$ on the right. The pressure $p = 10^5$ Pa is uniform in the entire domain as well as the velocity that is taken equal to $u = 1000$ m/s. The interface is initially located at $x_i = 0.4$ m. Fig. 4 shows computed results at time $t = 0.38$ ms. A mesh involving 100 computational cells is used. The second-order variant of the method is used with Superbee limiter. Symbols correspond to the numerical solution of the model while lines correspond to the exact solution. The interface is perfectly advected and the pressure and velocity fields are oscillation free. This test shows that the method is able to preserve mechanical equilibrium states in the presence of interfaces with very large density ratios.

### 5.2. Solid–solid shock tube with moderate pressure ratio

We consider a shock tube filled with solid aluminium with density $\rho = 2700 kg/m^3$ and shear modulus $\mu_s = 2.6 \times 10^{10}$ Pa initially at rest in the high pressure chamber ($p = 10^8$ Pa). The thermodynamic part of the aluminium is governed by the

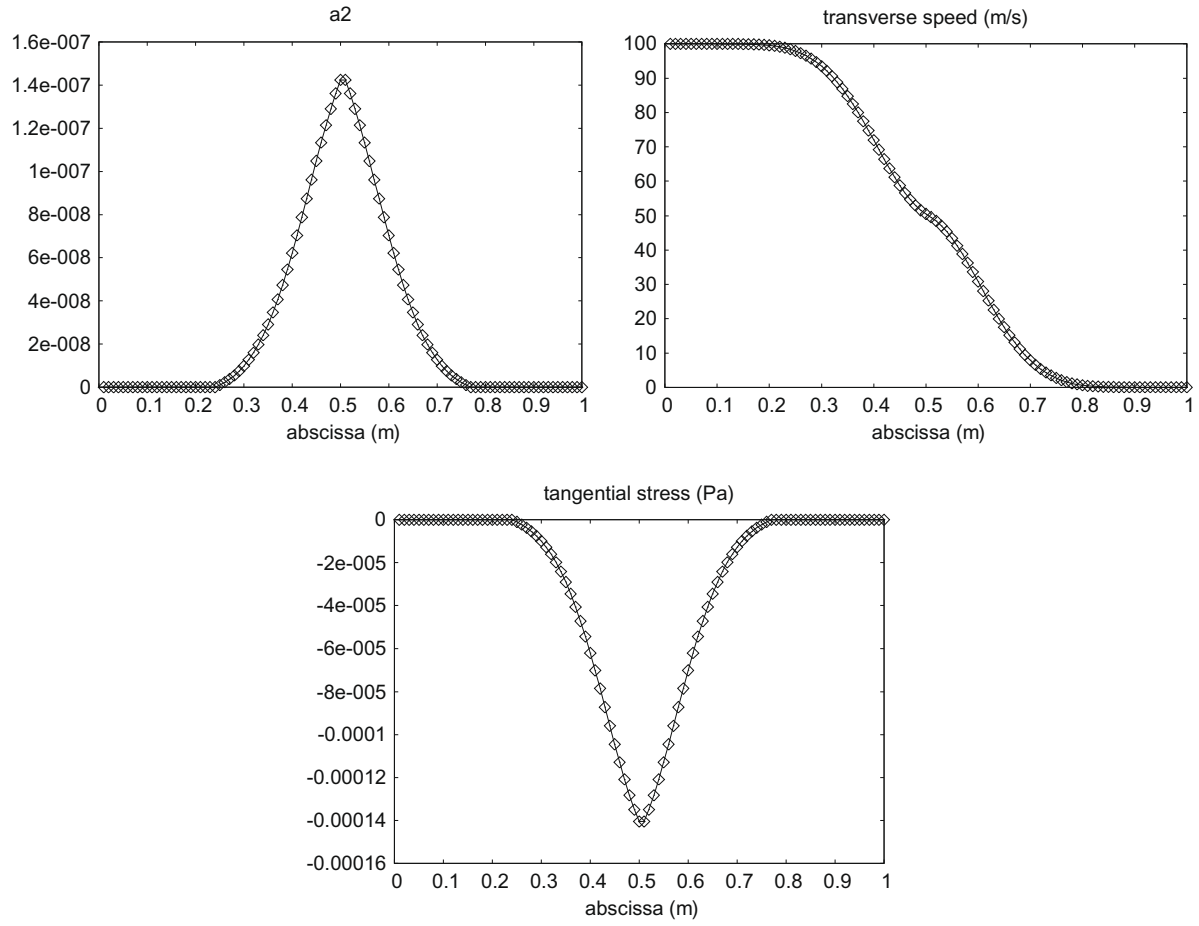


**Fig. 9.** Gas–gas interface with shear. An initial discontinuity of transverse velocity is imposed in a solid–gas mixture with a negligible amount of solid, at zero longitudinal velocity and atmospheric pressure. The diffuse interface model is unable to model sliding effects without specific correction.

stiffened gas equation with parameters $p_{\infty s} = 215.0 \times 10^8$ Pa and $\gamma_s = 3.4$. The low pressure chamber ($p = 10^5$ Pa) is filled with solid copper with density $\rho = 8900$ kg/m$^3$. The interface is initially located at $x_i = 0.5$ m. Fig. 5 shows computed results at time $t$ = 134 μs. A mesh involving 1000 computational cells is used. The second-order variant of the method is used with Minmod limiter. Symbols represent the numerical solution. A pressure jump is present at the interface but the normal stress $\sigma_{11}$ is clearly constant, as imposed by the interface conditions.

### 5.3. Solid–air shock tube with a high pressure ratio

We consider a shock tube with solid copper initially at rest in the high pressure chamber ($p = 5\ 10^9$ Pa) with density $\rho = 8900$ kg/m$^3$ and with air in the low pressure chamber ($p = 10^5$ Pa) with density $\rho = 50$ kg/m$^3$. The interface is initially located at $x_i = 0.6$ m. Fig. 6 shows computed results at time $t$ = 870 μs. A mesh involving 1000 computational cells is used. A second-order variant of the method is used with Minmod limiter. Lines represent the numerical solution of the model. These results show that the method is able to deal with very high pressure and density ratios at solid–gas interfaces.

### 5.4. Double expansion

We consider copper with small amount of air ($\alpha_g = 10^{-4}$). The tube is separated in two parts of equal lengths each part having different initial velocities. On the left part, the copper–air mixture is initially set into motion with the velocity −3000 m/s. The right part is set into motion with opposite velocity. The mixture is initially at atmospheric pressure and, the copper has the initial density $\rho = 8900$ kg/m$^3$ while the air has the density of $\rho = 1$ kg/m$^3$. Fig. 7 shows computed results at time $t$ = 88 μs with a mesh involving 2000 cells. The second-order version of the method with Minmod limiter is used. A "cavitation" pocket appears dynamically.

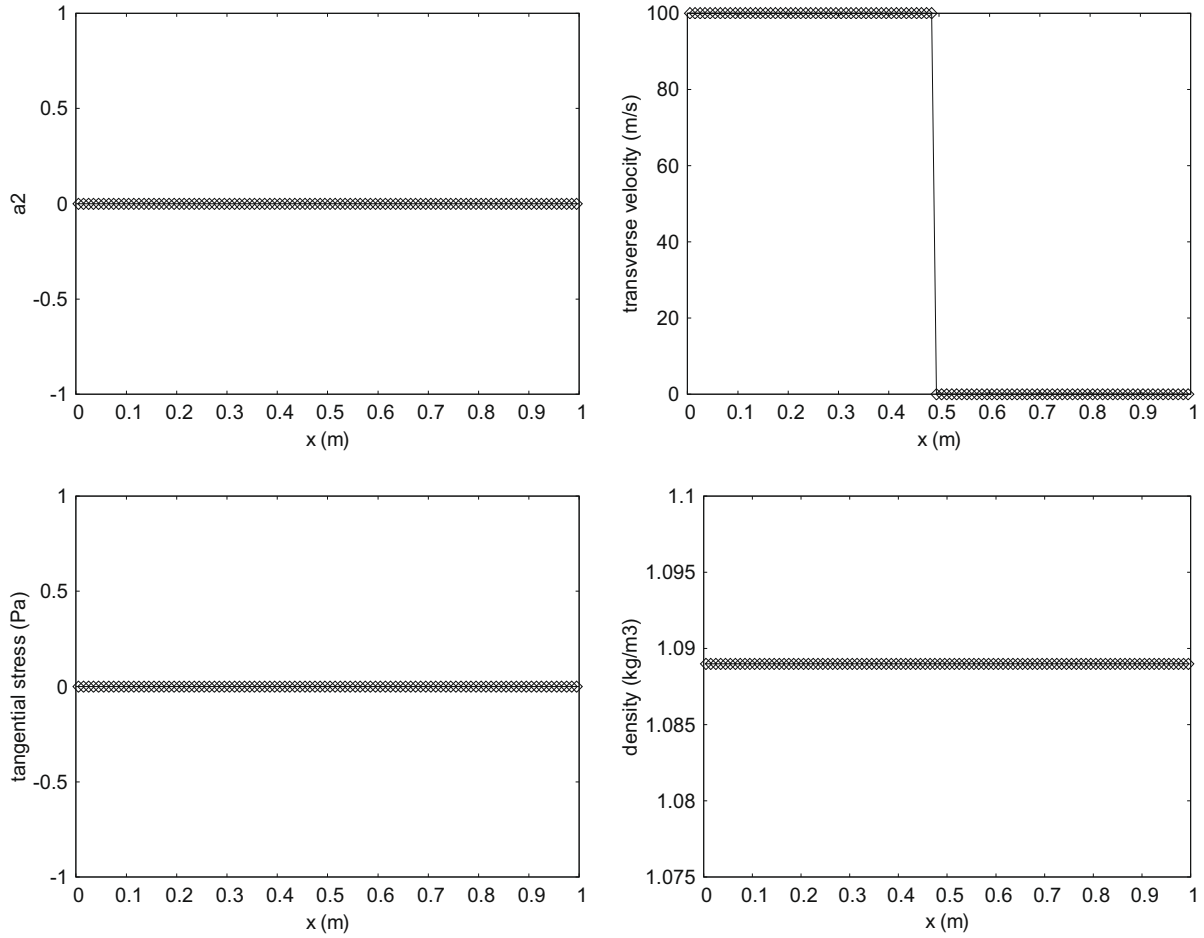


**Fig. 10.** Gas–gas interface with shear. An initial discontinuity of transverse velocity is imposed in a solid–gas mixture with a negligible amount of solid at zero longitudinal velocity and atmospheric pressure. The method now behaves correctly with sliding effects at gas–gas interfaces.

### 5.5. Solid–solid interface with shear

In presence of shear effects, five waves are expected to appear. We consider a "shock tube" filled with copper with a small amount of air ($\alpha_{air} = 10^{-6}$). An interface separates initially the high pressure chamber on the left where the copper–air mixture is at rest with pressure ($p = 10^8$ Pa) and the same mixture of materials on the right at low pressure ($p = 10^5$ Pa).

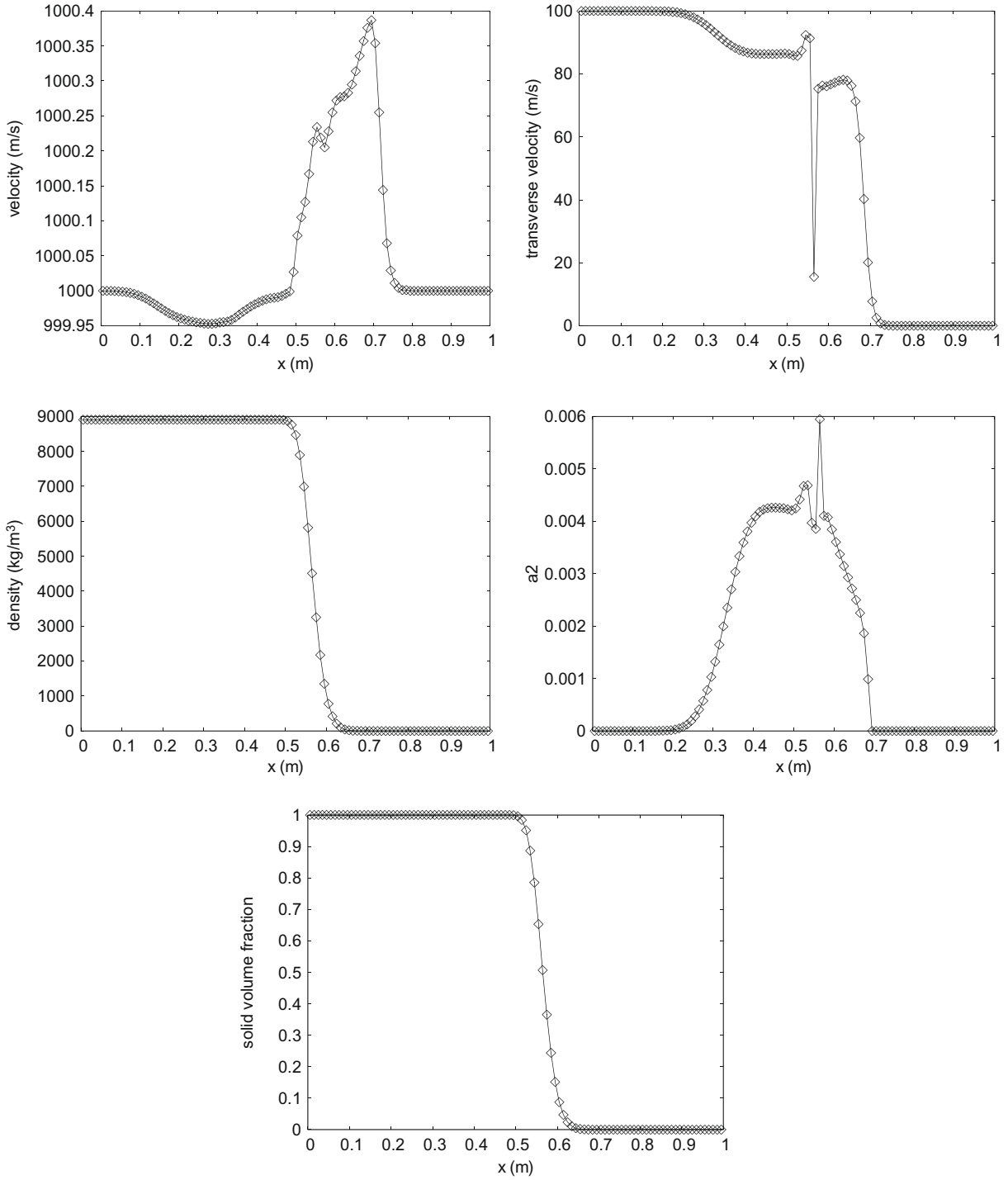


**Fig. 11.** Advection of a solid–gas interface at constant longitudinal velocity and at atmospheric pressure with a transverse velocity discontinuity. The numerical diffusion of the transverse velocity in the diffuse interface zone where the volume fraction varies creates tangential stress.

A tangential velocity discontinuity is imposed: $v = 0$ m/s on the left and $v = 100$ m/s on the right. The interface is initially located at $x_i = 0.5$ m. Fig. 8 shows computed results at time $t = 0.46$ ms. The single material results obtained with the pure solid model are compared with the present multimaterial model results and show perfect agreement. Both computations involve 1000 cells and use the second-order version of the method with Minmod limiter.

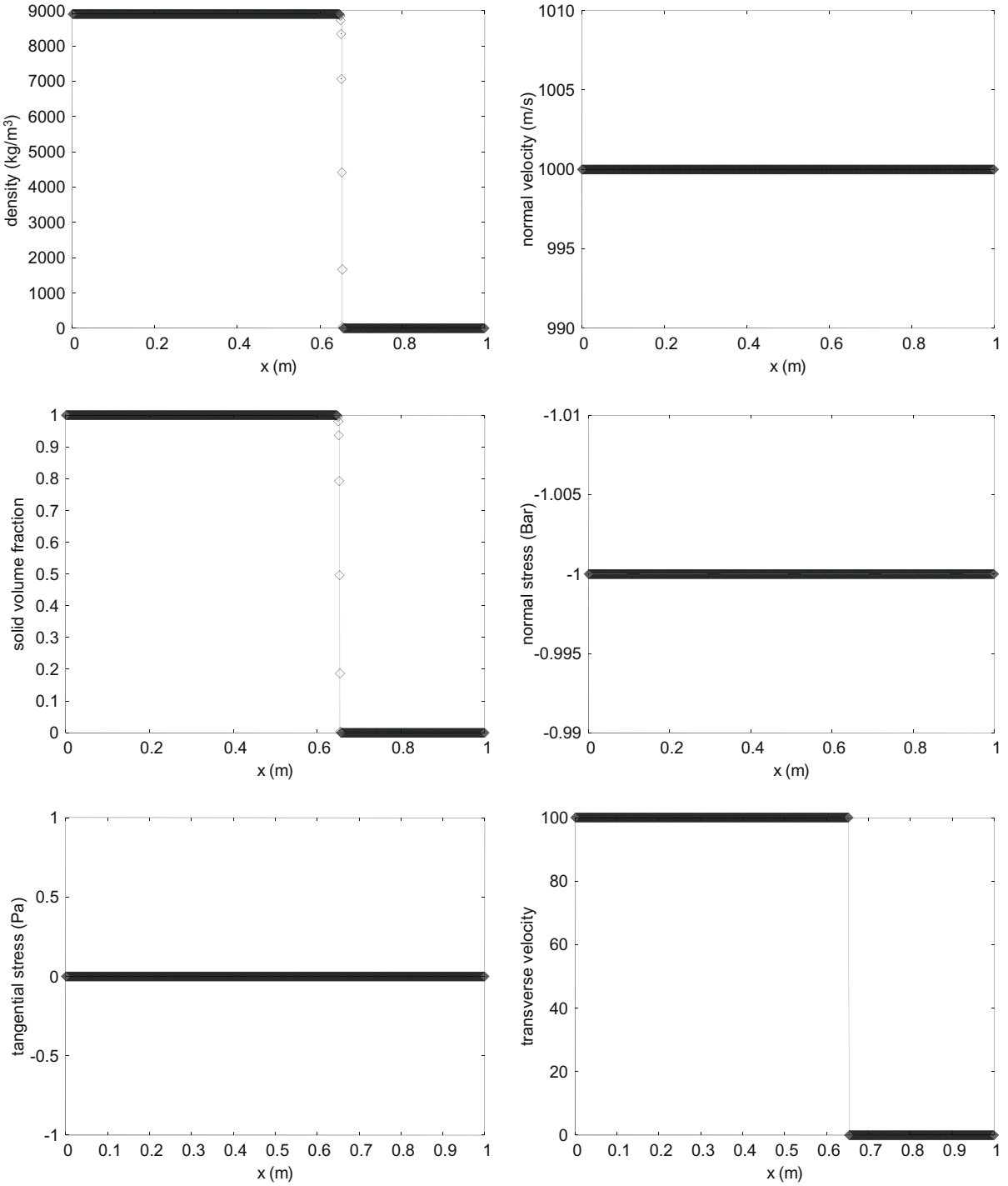


**Fig. 12.** Advection at constant longitudinal velocity in the presence of a tangential velocity discontinuity at a solid–gas interface. No tangential stress appears and the solution remains oscillation free.

It can be seen in Fig. 8 that the multiphase model perfectly fulfils the interface condition of continuity of tangential velocity at the solid–solid interface. This is no longer true for gas–gas interfaces and solid–gas interfaces.

### 5.6. Gas–gas interface with shear

To illustrate the difficulty in using the diffuse interface model when dealing with gas–gas interfaces in the presence of a transverse velocity discontinuity, let us take the same copper–air mixture as previously with reverse volume fractions ($\alpha_s = 10^{-7}$). Consequently, the flow is nearly pure gas.

The two parts of the tube are set to atmospheric pressure and zero longitudinal velocity. The only discontinuity corresponds to the transverse speed.

The corresponding results are shown with symbols in Fig. 9 at time $t = 2.97$ ms with lines. They are obtained with the first-order version of the method, employing a mesh involving 100 cells.

The main difference between solids and fluids is that the stress tensor is spherical for fluids while it is not for solids. As a consequence, the presence of a small amount of solid ($\alpha_s = 10^{-7}$) prevents sliding at the interface. Consequently, the tangential stress ($\sigma_{12}$) is non-zero, and this creates transverse waves in the gas phase, resulting in wrong wave structure in the vicinity of the interface.

This difficulty has been already mentioned when the interface solid–gas relations (58e) were discussed. We have to know what type of contact (solid–solid, fluid–fluid or solid–fluid) we are considering at a given interface. To do this, we add in the flow model a level set variable $\Phi$ defined initially by:

$$\Phi = \begin{cases} -1, & \text{if} \quad \alpha_s < 0.5, \\ 1, & \text{if} \quad \alpha_s > 0.5. \end{cases}$$

Function $\Phi$ is governed by the equation:

$$\frac{d\Phi}{dt} = 0,$$

and is approximated by the numerical scheme (60).

With this variable the Riemann problem solution is corrected with the following procedure:

$$\sigma_{12}^{*} = \begin{cases} \frac{(u_R - S_R)\rho_R(\alpha_s\sigma_{12s})_L - (u_L - S_L)\rho_L(\alpha_s\sigma_{12s})_R + (u_L - S_L)\rho_L(u_R - S_R)\rho_R(v_R - v_L)}{((u_R - S_R)\rho_R - (u - S_L)\rho_L)}, & \text{if} \quad \Phi_L > 0 \quad \text{and} \quad \Phi_R > 0, \\ 0, & \text{if} \quad \Phi_L < 0 \quad \text{or} \quad \Phi_R < 0. \end{cases}$$

The other variables in the Riemann problem solution are unchanged.

With this simple correction, the solid–solid and fluid–fluid single phase limits are preserved. The same test as in Fig. 9 is rerun with this correction and the results are shown in Fig. 10.

However, when dealing with solid–fluid interfaces, this correction is not enough as there is a non-linear coupling with the numerical diffusion of the volume fraction. This difficulty is illustrated in Fig. 11 where a solid–fluid interface is considered during transport at constant longitudinal velocity of 1000 m/s under atmospheric conditions. Computational results are obtained with the first-order scheme over a mesh involving 100 computational cells. The results are shown at time $t = 77$ μs.

The oscillations of the tangential stress are related to the numerical diffusion of the transverse velocity. They create non-physical stress waves in the solid.

To circumvent this supplementary difficulty, another correction is necessary as detailed in the next Section.

## 6. Ghost fluid method for transverse velocities

To enforce solid–fluid interface conditions, as presented previously, some choice has to be made regarding the correct set of jump relations for the transverse velocity given by (58e). This is done with an adaptation of the method due to Abgrall and

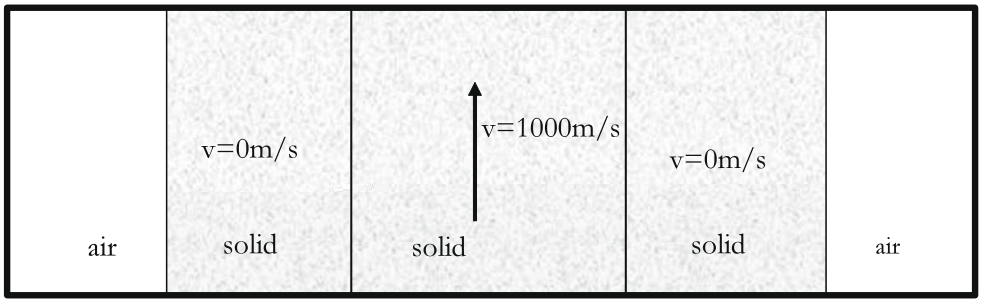


**Fig. 13.** Geometrical configuration for shear wave interaction with solid–air interfaces.

between the two cell centers $i$ and $i+1$. In this case two different fluxes and primitive variable vectors are computed after velocity extrapolation across the interface. In other words, this can be written as follows:If $\Phi_i^n \Phi_{i+1}^n > 0$ then $\mathbf{W}_{i+1/2}^* = \mathbf{W}^{HLLC}(\mathbf{V}_i^n, \mathbf{V}_{i+1}^n), \mathbf{F}_{i+1/2}^* = \mathbf{F}(\mathbf{W}_{i+1/2}^*)$If $\Phi_i^n \Phi_{i+1}^n < 0$ then

* Extrapolate the right tangential velocity to the left and solve the Riemann problem: $\mathbf{W}_{i+1/2,L}^* = \mathbf{W}^{HLLC}(\mathbf{V}_{L,i}^n, \mathbf{V}_{i+1}^n), \mathbf{F}_{i+1/2,L}^* = \mathbf{F}(\mathbf{W}_{i+1/2,L}^*)$.Variables $\mathbf{V}_{L,i}^n$has been changed with the tangential velocity component of the right state $\mathbf{V}_{i+1}^n$.
* Extrapolate the left tangential velocity to the right and solve the Riemann problem: $\mathbf{W}_{i+1/2,R}^* = \mathbf{W}^{HLLC}(\mathbf{V}_i^n, \mathbf{V}_{R,i+1}^n), \mathbf{F}_{i+1/2,R}^* = \mathbf{F}(\mathbf{W}_{i+1/2,R}^*)$Variables $\mathbf{V}_{R,i+1}^n$ has been changed with the tangential velocity component of the left state $\mathbf{V}_i^n$.

2. Following Farhat et al. [10] prediction of the solution is necessary to detect interfaces that may change cells during two consecutive time steps. A temporary value $\widetilde{\mathbf{V}}_i^{n+1}$of the solution is determined with:

$$\widetilde{\mathbf{V}}_i^{n+1} = \mathbf{V}_i^n + \frac{\Delta t}{\Delta x}\left((\mathbf{F}_{i-1/2,R}^* - \mathbf{F}_{i+1/2,L}^*) + \mathbf{H}_i^n(u_{i-1/2,R}^* - u_{i+1/2,L}^*) + \mathbf{K}_i^n\left(v_{i-1/2,R}^* - v_{i+1/2,L}^*\right)\right)$$

3. For each node $i$,If $\Phi_i^n \Phi_i^{n+1} > 0 \quad \mathbf{V}_i^{n+1} = \widetilde{\mathbf{V}}_i^{n+1}$If $\Phi_i^n \Phi_i^{n+1} < 0 \quad \mathbf{V}_i^{n+1} = \widetilde{\mathbf{V}}_i^{n+1}$ except the transverse speed $\tilde{v}_i^{n+1}$ that is taken to $v_i^R$ or $v_i^L$ depending on the flow direction.

### 6.1. Solid–air example with sliding

The test problem of Fig. 11 is rerun with the Ghost fluid correction in the diffuse interface method. We consider a tube filled with nearly pure solid copper on the left with a density $\rho_s = 8900$ kg/m$^3$ with a negligible amount of gas ($\alpha_g = 10^{-7}$) at density $\rho_g = 1$ kg/m$^3$. On the right of the initial discontinuity, located at $x_i = 0.5$ m, the same mixture is considered with reversed proportions ($\alpha_s = 10^{-7}$). Both chambers are set at atmospheric pressure with an initial longitudinal velocity of $u = 1000$ m/s. A tangential velocity discontinuity of 100 m/s is present. Computed results are shown in Fig. 12 at time $t = 0.15$ ms. Symbols correspond to the numerical solution and lines to the exact solution. A mesh involving 1000 cells is used and the solution is evolved with the second-order variant of the method with Superbee limiter. The interface is well transported and the pressure and velocity fields are oscillation free.

### 6.2. Shear in solid in the presence of solid–gas interfaces

In this test case, two solid–gas interfaces (located initially at $x_i = 0.15m$ and $x_i = 0.85m$) are present. A part of the solid phase is set in transverse motion (Fig. 13). All materials have initial zero longitudinal velocity and atmospheric pressure. The initial physical parameters are the same as previously.

The initial transverse velocity discontinuity produces shear waves that propagate in the direction of solid–air interfaces. At each interface, there is a wave diffraction and a reflected shear wave propagates in the solid. Numerical resolution of this test requires a correct and clear treatment of material interfaces.

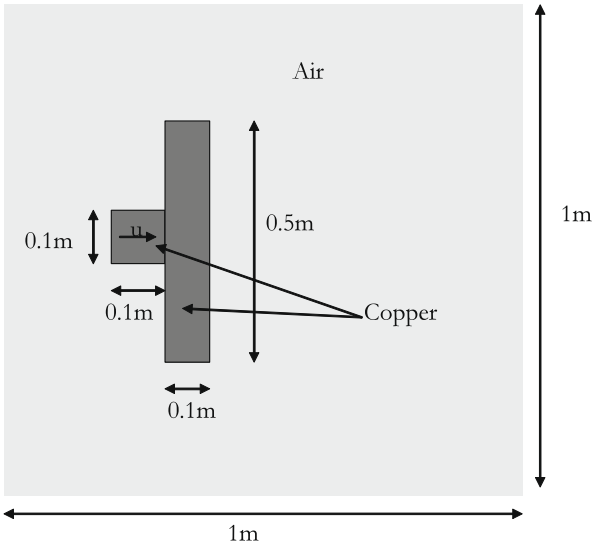


**Fig. 15.** Initial configuration for the copper impact test. The initial velocity of the impactor (on the left) is $u = 800$ m/s, the numerical computation involves $1000 \times 1000$ cells.

Results are shown in Fig. 14 at instants $t = 5.46$ μs (before wave interaction with interfaces, at the left) and $t = 18$ μs (after wave interaction with interfaces, at the right). Also, the convergence analysis is performed by using 100 (symbols), 1000 (thick lines) and 10,000 (thin lines) mesh cells with a second-order Godunov method.

## 7. Multi-dimensional examples

Multi-dimensional extension of the method follows the lines of Saurel et al. [30] with preceding extensions. We present hereafter some computational examples showing the capabilities of the present diffuse interface method for the solid–fluid interaction under extreme deformations.

### 7.1. Impact of a projectile on a solid plate

We consider here an impact of a solid projectile on a solid plate for different values of shear modulus. The projectile has the initial velocity $u = 800$ m/s while the plate and the surrounding air are at rest. This projectile is a square of 0.1 m length. The plate is 0.5 m long and 0.1 m width. The contact between the plate and the projectile is already done at initial time. The other part of the computational domain contains a compressible fluid (air at atmospheric conditions). The physical domain is 1 m long and 1 m high. The mesh contains 1000 cells along $x$ and $y$ directions. Fig. 15 shows the initial configuration. The

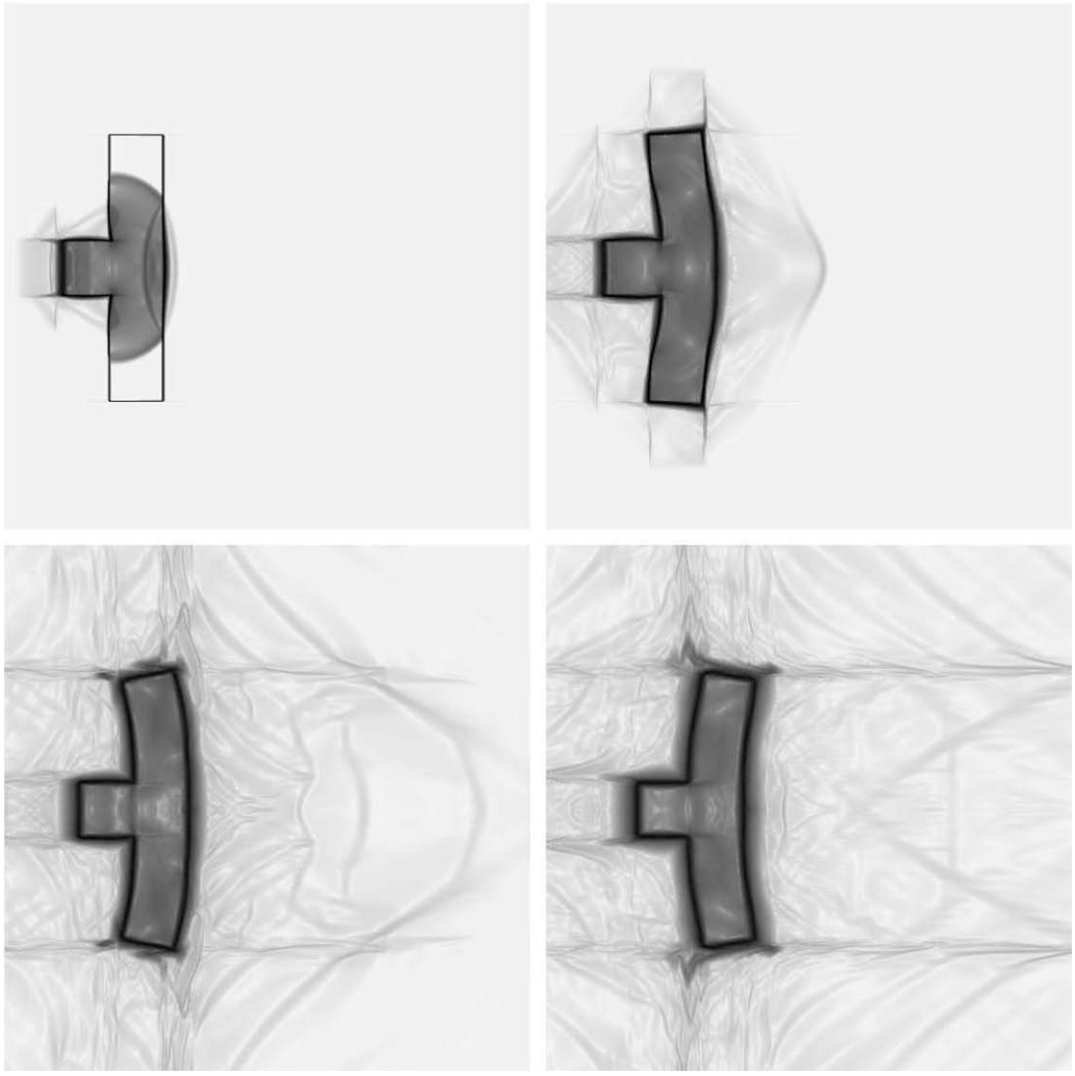

**Fig. 16.** Impact at 800 m/s of a copper projectile on a copper plate at rest surrounded by air at atmospheric pressure. The schlieren image of the density is represented for time $t = 3.6 \times 10^{-5}$ s, $t = 1.06 \times 10^{-4}$ s, $t = 3.2 \times 10^{-4}$ s and $t = 6.09\ 10^{-4}$ s. Numerical computations involve $1000 \times 1000$ cells using a second-order Godunov method with Minmod limiter. The plate oscillates during time evolution.

parameters of the solid are as follows: $\gamma_s = 4.22, p_{\infty s} = 342.0 \times 10^8$ Pa and the density $\rho_s = 8900$ kg/m$^3$. The following results are presented for different shear modulus: $\mu_s = 9.2 \times 10^{10}$ Pa corresponding to real copper at ambient temperature, $\mu_s = 1.0 \times 10^9$ corresponding to a softer material, and $\mu_s = 0$ corresponding to the fluid limit. The air is considered as ideal gas with parameters $\gamma_g = 1.4$ and a density $\rho_g = 1$ kg/m$^3$. Initially, a small amount of air ($\alpha_g = 10^{-4}$) is present in the solid, and a small amount of the solid is present in the air ($\alpha_s = 10^{-4}$). All the results presented hereafter are obtained with a second-order Godunov method using Minmod limiter.

First, we take $\mu_s = 9.2 \times 10^{10}$ Pa that corresponds copper parameters. The solution is shown at time $t = 3.6 \times 10^{-5}$ s,$t = 1.06 \times 10^{-4}$ s,$t = 3.2 \times 10^{-4}$ s and $t = 6.09\ 10^{-4}$ s. As we can see in Fig. 16, the solid plate oscillates, while shock waves propagate in the air.

Then, we consider a solid with $\mu = 1.0 \times 10^9$ Pa. The solution is represented at times $t = 3.5 \times 10^{-5}$ s,$t = 1.4 \times 10^{-4}$ s,$t = 4.2 \times 10^{-4}$ s and $t = 7.1 \times 10^{-4}$ s. As we can see in Fig. 17, the solid is really bent. The strain is limited by elasticity and the wave are well propagated in both materials. Some filaments appears in the vicinity of the solid–gas interface. These filaments are linked to the numerical treatment of the sliding between fluid and solid (a part of the diffusion zone can slide from the solid part). The sharper will be the interface, the less solid will be removed from the interfaces.

Then, we consider the fluid limit: $\mu = 0$ Pa. The solution is represented at time $t = 7.5 \times 10^{-5}$ s,$t = 1.87 \times 10^{-4}$ s,$t = 6 \times 10^{-4}$ s and $t = 1.03 \times 10^{-3}$ s. As shown in Fig. 18, the solid (which is considered as a fluid) is really bent. The strain

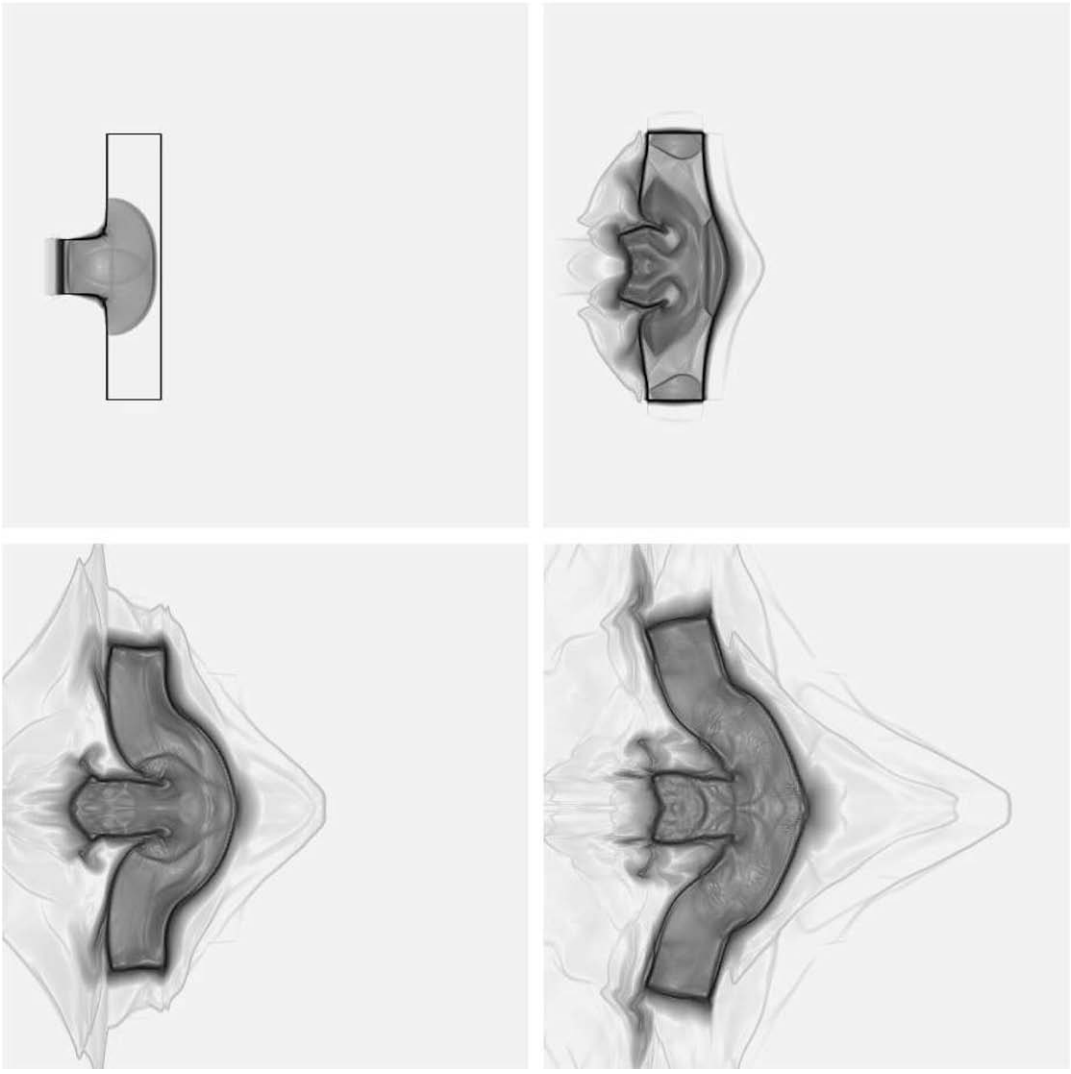

**Fig. 17.** Impact at 800 m/s of a copper projectile on copper plate with $\mu = 1. \times 10^9$ Pa at rest surrounded by air at atmospheric pressure. The schlieren image of the density is represented for time $t = 3.5 \times 10^{-5}$ s,$t = 1.4 \times 10^{-4}$ s,$t = 4.2 \times 10^{-4}$ s and $t = 7.1 \times 10^{-4}$ s. Numerical computations involve $1000 \times 1000$ cells using a second-order method using the Minmod limiter. The plate is really bent but the strain stays limited.

increases, filaments appear on the side of the projectile and propagate to infinity. The material does not turn back to its initial configuration.

As it can be seen in Figs. 16–18 the material behavior depends strongly on $\mu_s$.

### 7.2. Impact of cylinders

The numerical code we used to study the plane 2D problems can easily be adapted to axisymmetric 2D problems. Without going into details we present here some numerical results. Consider a highly deformable cylinder impacting a rigid surface (see Fig. 19). Usually, comparisons are done with metal projectile impacts Wilkins and Guinan [38] and Howell and Ball [19]. However, when dealing with metals, plastic transformation occurs and considerably modifies the interface dynamics. We made a comparison with experimental results on the impacting of cylindrical gel samples (cylindrical drops of jelly-like materials). Jelly-like materials remain elastic even for extreme deformations (between 100% and 200% ). This regime was recently studied experimentally by Luu and Forterre [22]. A cylindrical gel sample (carbopol) of diameter $L_0$ impacting a rigid hydrophobic surface, first spreads over the surface until some limit size $L_M$ and then a full elastic recoil is observed which may be followed by a complete rebound. We reproduced this quasi-reversible behavior numerically. The separate form of the energy Eq. (9) was also used with $\mu_s = 85Pa$. The comparison during the spreading phase at a given time instant is shown in Fig. 20. Also, the Fig. 21 shows the dependence of the relative stretching $(L_M - L_0)/L_0$ as a function of the Mach number $M$

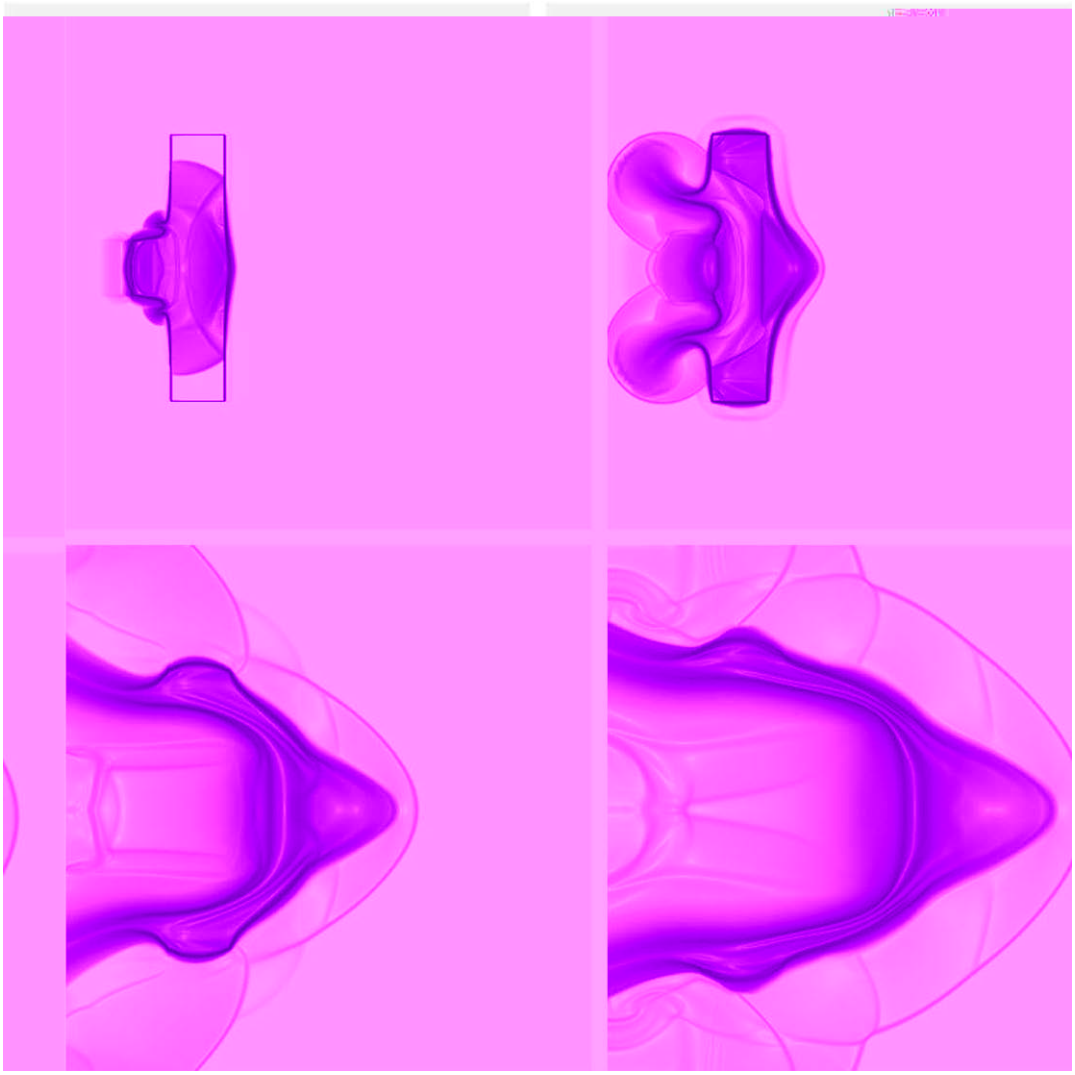

**Fig. 18.** Impact at 800 m/s of a copper projectile on copper plate with $\mu = 0$ at rest surrounded by air at atmospheric pressure. The schlieren image of the density is represented for time $t = 7.5 \times 10^{-5}$ s,$t = 1.87 \times 10^{-4}$ s,$t = 6 \times 10^{-4}$ s and $t = 1.03 \times 10^{-3}$ s. Numerical computations involve $1000 \times 1000$ cells using a second-order method with Minmod limiter. The plate is really bent, filaments appear and propagate to infinity.

which is the ratio of the impact velocity $v_0$ to the velocity of transversal waves (the Mach number can be very large, because the shear modulus of the carbopol is small). The squares correspond to the experimental data, the triangles correspond to

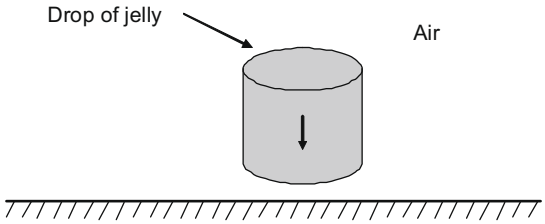


**Fig. 19.** A cylindrical drop of jelly is impacting a rigid surface.

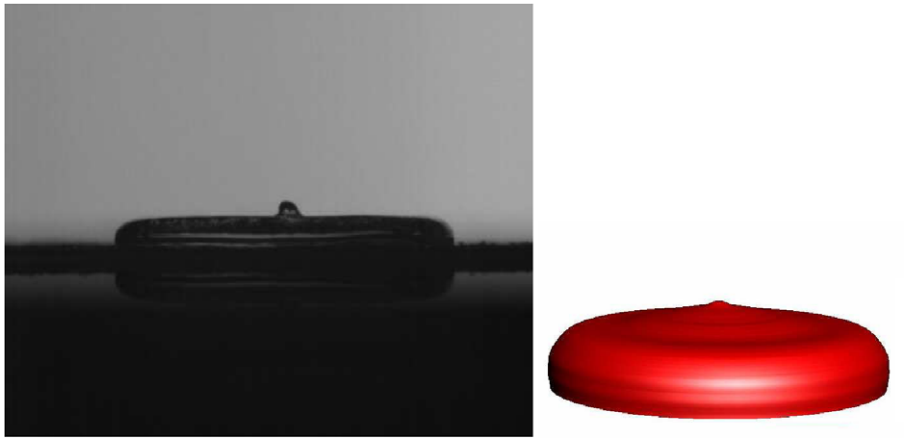

**Fig. 20.** Comparison of the spreading phase of the cylinder impacting a rigid surface. Experiments by Luu and Forterre [22] are shown on the left, computed results are shown on the right.

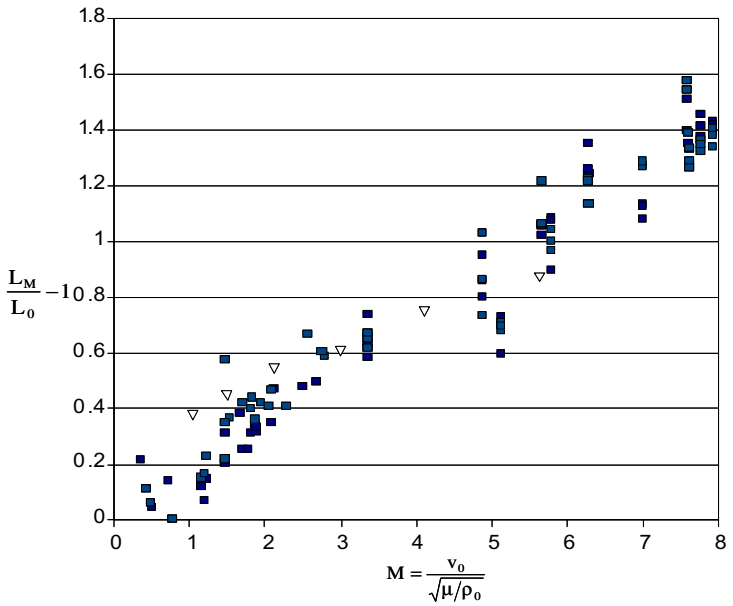


**Fig. 21.** Relative deformation versus the elastic Mach number for carbopol drops falling on a glass surface, measured in experiments (squares) and predicted by the model (triangles).

numerical results. Overall, the correspondence is quite good. A detailed study of this interesting quasi-reversible phenomena will be published in a forthcoming paper.

## 8. Conclusions and perspectives

A hyperbolic diffuse interface model for elastic solid–fluid coupling in Eulerian formulation has been developed in conjunction with an appropriate numerical method. Model's capabilities are illustrated on two-dimensional hypervelocity impacts of solids (plane and axisymmetric geometry). Extra work is necessary to introduce plasticity effects to confront the model with real physical experiments of metal's impact. This work is in progress.

## Acknowledgments

The authors have been partially supported by Grant No. 07.34.048 from DGA. The authors thank anonymous referees for important remarks and suggestions.

## Appendix A. Derivation of the phase specific volume relation in the relaxation method

The phase's energy equations used during the pressure relaxation step read:

$$e_k - e_k^i + \hat{p}_I(\tau_k - \tau_k^i) = 0, \quad k = 1, 2,$$

where $e_k = \varepsilon_k^h + \varepsilon_k^e = \varepsilon_k^h(p_k, \rho_k) + \varepsilon_k^e(A^{(1)}, A^{(2)}, B^{(1)}, B^{(2)})$. If $k = g$, $\varepsilon_g^e = 0$ since $\mu_g = 0$. To simplify the notations, we do not use here index "$f$" for a final equilibrium state, and we denote

$$p = p_1^f = p_2^f = \hat{p}_I.$$

Using the stiffened gas EOS for the hydrodynamic part and the elastic EOS the energy equations become:

$$\frac{p + \gamma_s p_{\infty,s}}{\rho_s(\gamma_s - 1)} + \left(\frac{\mu_s}{4\rho_{s0}} tr\left(\left(\frac{\langle G\rangle}{|\langle G\rangle|^{1/3}} - I\right)^2\right)\right) - \frac{p_s^i + \gamma_k p_{\infty,s}}{\rho_s^i(\gamma_s - 1)} - \left(\frac{\mu_s}{4\rho_{s0}} tr\left(\left(\frac{\langle G\rangle}{|\langle G\rangle|^{1/3}} - I\right)^2\right)\right)^i + p(\tau_s - \tau_s^i) = 0.$$

This equation can be simplified because during the relaxation process the tensor $\langle G\rangle/|\langle G\rangle|^{1/3}$ does not change. Indeed, during this step

$$\begin{aligned} A^{(1)} &= (A^{(1)})^i, \\ A^{(2)} &= (A^{(2)})^i, \\ B^{(1)} &= (B^{(1)})^i, \\ B^{(2)} &= (B^{(2)})^i, \end{aligned}$$

Consequently:

$$tr\left(\left(\frac{\langle G\rangle}{|\langle G\rangle|^{1/3}} - I\right)^2\right) = tr\left(\left(\frac{\langle G\rangle}{|\langle G\rangle|^{1/3}} - I\right)^2\right)^i.$$

It results that the phase energy equations for both solid and gas phases reduce to:

$$\frac{p + \gamma_k p_{\infty k}}{\rho_k(\gamma_k - 1)} - \frac{p_k^i + \gamma_k p_{\infty k}}{\rho_k^i(\gamma_k - 1)} + p(\tau_k - \tau_k^i) = 0, \quad k = s, g.$$

The phase specific volume as a function of the relaxed pressure, when the stiffened gas EOS is used thus reads:

$$\tau_k(p) = \tau_k^i \frac{p_k^i + \gamma_k p_{\infty k} + (\gamma_k - 1)p}{p + \gamma_k p_{\infty k} + (\gamma_k - 1)p}, \quad k = s, g.$$

## Appendix B. Second-order extension of the hyperbolic solver

The second-order extension of the Godunov type method we use consists in applying the following MUSCL algorithm [36]:

- Gradients limitation
  In a cell $i$, at instant $n$, primitive variables $\mathbf{W}_i^n$ of formulation (47) are known. Let us denote by $\Delta_i^-$ and $\Delta_i^+$ the primitive variables gradients on the left and right boundary of cell $i$ respectively. They are defined by:
  $$\Delta_i^- = \frac{\mathbf{W}_i^n - \mathbf{W}_{i-1}^n}{\Delta x} \quad \text{and} \quad \Delta_i^+ = \frac{\mathbf{W}_{i+1}^n - \mathbf{W}_i^n}{\Delta x}$$
- Limitation
  A slope limiter function $\xi$ ensures the stability of the scheme and allows the calculation of slopes $\Delta_i$ in the cell $i$. A large number of slope limiters are available in the literature (Minmod, Van Leer or Superbee, etc.).In each cell the slope $\Delta_i = \xi(\Delta_i^-, \Delta_i^+)$ is computed regarding all variables, except the geometrical variables $(A^{(1)}, A^{(2)}, B^{(1)}, B^{(2)})$ for which the slopes $\Delta_i$ are taken equal to zero.
- Variables extrapolation
  With the preceding slope vector $\Delta_i$ it is possible to compute the extrapolated primitive variable vectors $\mathbf{W}_{i,L}$ and $\mathbf{W}_{i,R}$, respectively corresponding to the left and right boundary of cell $i$. We have:
  $$\mathbf{W}_{i,L}^n = \mathbf{W}_i^n - \frac{\Delta x}{2}\Delta_i \quad \text{and} \quad \mathbf{W}_{i,R}^n = \mathbf{W}_i^n + \frac{\Delta x}{2}\Delta_i.$$
- Evolution over a half time step
  The second-order time accuracy consists in using the following primitive variables scheme:
  $$\mathbf{W}_i^{n+1/2} = \mathbf{W}_i^n + \frac{1}{2}\frac{\Delta t}{\Delta x}\mathbf{A}_i^n\left[\mathbf{W}_{i,L}^n - \mathbf{W}_{i,R}^n\right].$$
  From the evolution at the cell center, the cell boundary variables are deduced at the same time:
  $$\mathbf{W}_{i,L}^{n+1/2} = \mathbf{W}_i^{n+1/2} - \frac{\Delta x}{2}\Delta_i \quad \text{and} \quad \mathbf{W}_{i,R}^{n+1/2} = \mathbf{W}_i^{n+1/2} + \frac{\Delta x}{2}\Delta_i.$$
- Riemann problem resolution
  The Riemann problem is now computed on each cell boundaries using extrapolated variables at the half time step $\mathbf{W}_{i,L,R}^{n+1/2}$. The flux vector of formulations (59) and (60) as well as inter-cell velocity components are computed.
- Classical evolution over the entire time step:
  Numerical schemes (59) and (60) are used with inter-cell variables and fluxes computed previously.

## Appendix C. Explicit form of EOS for the solid component

The partial elastic energy of the solid is:

$$\begin{aligned}\alpha_s\rho_s\varepsilon_s^e &= \frac{\mu_s}{4|\langle G\rangle|^{1/6}}tr((\langle G\rangle - |\langle G\rangle|^{1/3}I)^2)\\ &= \frac{\mu_s}{4|\langle G\rangle|^{1/6}}\left(\left(1-|\langle G\rangle|^{1/3}\right)^2 + \left(\left(A^{(1)}\right)^2 + \left(A^{(2)}\right)^2 - |\langle G\rangle|^{1/3}\right)^2\right.\\ &\quad \left. + \left(\left(B^{(1)}\right)^2 + \left(B^{(2)}\right)^2 - |\langle G\rangle|^{1/3}\right)^2 + 2\left(A^{(1)}B^{(1)} + A^{(2)}B^{(2)}\right)^2\right),\end{aligned}$$

where

$$\langle G\rangle = \begin{pmatrix} (A^{(1)})^2 + (A^{(2)})^2 & A^{(1)}B^{(1)} + A^{(2)}B^{(2)} & 0\\ A^{(1)}B^{(1)} + A^{(2)}B^{(2)} & (B^{(1)})^2 + (B^{(2)})^2 & 0\\ 0 & 0 & 1\end{pmatrix},$$

and

$$|\langle G\rangle| = (A^{(1)}B^{(2)} - A^{(2)}B^{(1)})^2.$$

The components of the averaged solid stress tensor are:

$$\begin{aligned}\alpha_s\sigma_{11s} &= -\alpha_s p_s - \frac{\mu_s}{3}\left(\frac{2((A^{(1)})^2 + (A^{(2)})^2)^2 + (A^{(1)}B^{(1)} + A^{(2)}B^{(2)})^2 - ((B^{(1)})^2 + (B^{(2)})^2)^2 - 1}{|\langle G\rangle|^{1/6}}\right)\\ &\quad + \frac{\mu_s}{3}|\langle G\rangle|^{1/6}\left(2\left(A^{(1)}\right)^2 + 2(A^{(2)})^2 - (B^{(1)})^2 - (B^{(2)})^2 - 1\right),\\ \alpha_s\sigma_{12s} &= -\mu_s(A^{(1)}B^{(1)} + A^{(2)}B^{(2)})\left(\frac{(A^{(1)})^2 + (A^{(2)})^2 + (B^{(1)})^2 + (B^{(2)})^2}{|\langle G\rangle|^{1/6}} - |\langle G\rangle|^{1/6}\right).\end{aligned}$$

The components of the averaged gas stress tensor are:

$$\sigma_{11g} = -p_g,$$
$$\sigma_{12g} = 0.$$

## References


[1] R. Abgrall, How to prevent pressure oscillations in multicomponent flow calculations: a quasi-conservative approach, J. Comput. Phys. 125 (1996) 150–160.
[2] R. Abgrall, S. Karni, Computations of compressible multifluids, J. Comput. Phys. 169 (2) (2001) 594–623.
[3] R. Abgrall, R. Saurel, Discrete equations for physical and numerical multiphase mixtures, J. Comput. Phys. 186 (2) (2003) 361–396.
[4] D.P. Babii, S.K. Godunov, V.T. Zhukov, O.B. Feodoritova, On the difference approximations of overdetermined hyperbolic equations of classical mathematical physics, Comput. Math. Math. Phys. 47 (3) (2007) 427–441.
[5] M. Baer, J. Nunziato, A two-phase mixture theory for the deflagration-to-detonation transition (DDT) in reactive granular materials, Int. J. Multiphase Flows 12 (1986) 861–889.
[6] Y. Chen, J. Glimm, D. Sharp, Q. Zhang, A two-phase flow model of the Rayleigh–Taylor mixing zone, Phys. Fluid 8 (1996) 816–825.
[7] A. Chinnayya, E. Daniel, R. Saurel, Modeling detonation waves in heterogeneous energetic materials, J. Comput. Phys. 196 (2) (2004) 490–538.
[8] G.-H. Cottet, E. Maitre, T. Milcent, Eulerian formulation and level set models for incompressible fluid-structure interaction, Math. Modell. Numer. Anal. 42 (3) (2008) 471–492.
[9] S.F. Davis, Simplified second-order Godunov-type methods, SIAM J. Sci. Stat. Comput. 9 (1988) 445–473.
[10] C. Farhat, A. Rallu, S. Shankaran, A higher-order generalized ghost fluid method for the poor for the three-dimensional two-phase flow, Comput. Underwater Implos. J. Comput. Phys. 227 (2008) 7674–7700.
[11] R. Fedkiw, Coupling an Eulerian fluid calculation to a Lagrangian solid calculation with the ghost fluid method, J. Comput. Phys. 175 (2002) 200–224.
[12] S. Gavrilyuk, R. Gouin, A new form of governing equations of fluids arising from Hamilton's principle, Int. J. Eng. Sci. 37 (1999) 1495–1520.
[13] S. Gavrilyuk, R. Saurel, Mathematical and numerical modeling of two-phase compressible flows with micro-inertia, J. Comput. Phys. 175 (2002) 326–360.
[14] S. Gavrilyuk, N. Favrie, R. Saurel, Modelling wave dynamics of compressible elastic materials, J. Comput. Phys. 227 (2008) 2941–2969.
[15] J. Glimm, D. Saltz, D. Sharp, Two-phase modelling of a fluid mixing layer, J. Fluid Mech. 378 (1999) 119–143.
[16] S.K. Godunov, Elements of Continuum Mechanics, Nauka, Moscow, 1978 (in Russian).
[17] S.K. Godunov, E.I. Romenskii, Elements of Continuum Mechanics and Conservation Laws, Kluwer Academic Plenum Publishers, NY, 2003.
[18] C.W. Hirt, B.D. Nichols, Volume of fluid (VOF) method for the dynamics of free boundaries, J. Comput. Phys. 39 (1) (1981) 201–225.
[19] B.P. Howell, G.J. Ball, A free-Lagrange augmented Godunov method for the simulation of elastic–plastic solids, J. Comput. Phys. 175 (2002) 128–167.
[20] A. Kapila, R. Menikoff, J. Bdzil, S. Son, D. Stewart, Two-phase modeling of DDT in granular materials: reduced equations, Phys. Fluid 13 (2001) 3002–3024.
[21] O. Le Metayer, J. Massoni, R. Saurel, Modelling evaporation fronts with reactive Riemann solvers, J. Comput. Phys. 205 (2005) 567–610.
[22] L.-H. Luu, Y. Forterre, Drop impact of yield-stress fluids, J. Fluid Mech., accepted for publication.
[23] G.H. Miller, P. Colella, A high-order Eulerian Godunov method for elastic–plastic flow in solids, J. Comput. Phys. 167 (2001) 131–176.
[24] G.H. Miller, P. Colella, A conservative three-dimensional Eulerian method for coupled fluid–solid shock capturing, J. Comput. Phys. 183 (2002) 26–82.
[25] A. Murrone, H. Guillard, A five equation reduced model for compressible two-phase flow problems, J. Comp. Phys. 202 (2005) 664–698.
[26] F. Petitpas, E. Franquet, R. Saurel, O. LeMetayer, A relaxation–projection method for compressible flows Part II: The artificial heat exchange for multiphase shocks, J. Comp. Phys. 225 (2007) 2214–2248.
[27] J.N. Plohr, B.J. Plohr, Linearized analysis of Richtmyer–Meshkov flow for elastic materials, J. Fluid Mech. 537 (2005) 55–89.
[28] R. Saurel, R. Abgrall, A multiphase Godunov method for compressible multifluid and multiphase flows, J. Comput. Phys. 150 (1999) 425–467.
[29] R. Saurel, O. Le Metayer, A multiphase model for interfaces, shock, detonation waves and cavitation, J. Fluid Mech. 431 (2001) 239–271.
[30] R. Saurel, F. Petitpas, R.A. Berry, Simple and efficient relaxation method for interfaces separating compressible fluids cavitating flows and shock in multiphase mixtures, J. Comp. Phys. 228 (2009) 1678–1712.
[31] R. Saurel, S. Gavrilyuk, F. Renaud, A multiphase model with internal degrees of freedom: application to shock–bubble interaction, J. Fluid Mech. 495 (2003) 283–321.
[32] J. Serrin, Mathematical principles of classical fluid dynamics, Encyclopedia of Physics, vol. 13, Springer-Verlag, 1959. I.
[33] H. Stewart, B. Wendroff, Two-phase flows: models and methods, J. Comput. Phys. 56 (1984) 363–409.
[34] E.F. Toro, M. Spruce, W. Speares, Restoration of the contact surface in the HLL-Riemann Solver, Shock Waves 4 (1994) 25–34.
[35] E.F. Toro, Riemann Solvers and Numerical Methods for Fluid Dynamics: A Practical Introduction, second ed., Springer-Verlag, 1999.
[36] B. Van Leer, Towards the ultimate conservative difference scheme IV. A new approach to numerical convection, J. Comput. Phys. 23 (1979) 276–299.
[37] M.L. Wilkins, Calculation of elastic–plastic flow, in: B. Alder et al. (Eds.), Methods of Computational Physics, vol. 3, Academic Press, NY, 1964.
[38] M.L. Wilkins, M.W. Guinan, Impact of cylinders on a rigid boundary, J. Appl. Phys. 44 (3) (1973) 1200–1206.